



## GrSMBMIP: Intercomparison of the modelled 1980-2012 surface mass balance over the Greenland Ice sheet

Xavier Fettweis<sup>1</sup>, Stefan Hofer<sup>1,2</sup>, Uta Krebs-Kanzow<sup>3</sup>, Charles Amory<sup>1</sup>, Teruo Aoki<sup>4,5</sup>, Constantijn J. Berends<sup>6</sup>, Andreas Born<sup>7,8</sup>, Jason E. Box<sup>9</sup>, Alison Delhasse<sup>1</sup>, Koji Fujita<sup>10</sup>, Paul Gierz<sup>3</sup>, Heiko Goelzer<sup>6,11</sup>,  
5 Edward Hanna<sup>12</sup>, Akihiro Hashimoto<sup>4</sup>, Philippe Huybrechts<sup>13</sup>, Marie-Luise Kapsch<sup>14</sup>, Michalea D. King<sup>15</sup>,  
Christoph Kittel<sup>1</sup>, Charlotte Lang<sup>1</sup>, Peter L. Langen<sup>16,17</sup>, Jan T. M. Lenaerts<sup>18</sup>, Glen E. Liston<sup>19</sup>, Gerrit  
Lohmann<sup>3</sup>, Sebastian H. Mernild<sup>20,21,22,23</sup>, Uwe Mikolajewicz<sup>14</sup>, Kameswarrao Modali<sup>14</sup>, Ruth H.  
Mottram<sup>16</sup>, Masashi Niwano<sup>4</sup>, Brice Noël<sup>6</sup>, Jonathan C. Ryan<sup>24</sup>, Amy Smith<sup>25</sup>, Jan Streffing<sup>3</sup>, Marco  
Tedesco<sup>26</sup>, Willem Jan van de Berg<sup>6</sup>, Michiel van den Broeke<sup>6</sup>, Roderik S. W. van de Wal<sup>6, 27</sup>, Leo van  
10 Kampenhout<sup>6</sup>, David Wilton<sup>28</sup>, Bert Wouters<sup>29</sup>, Florian Ziemen<sup>14</sup>, Tobias Zolles<sup>7,8</sup>

<sup>1</sup>University of Liège, Department of Geography, Belgium.

<sup>2</sup>School of Geographical Sciences, University of Bristol, UK.

<sup>3</sup>Alfred-Wegener-Institut, Helmholtz Centre for Polar and Marine Research, Bremerhaven, Germany.

<sup>4</sup>Meteorological Research Institute, Japan Meteorological Agency, Tsukuba, Japan.

15 <sup>5</sup>National Institute of Polar Research, Tachikawa, Japan.

<sup>6</sup>Institute for Marine and Atmospheric research Utrecht, Utrecht University, The Netherlands.

<sup>7</sup>Department of Earth Science, University of Bergen, Bergen, Norway.

<sup>8</sup>Bjerknes Centre for Climate Research, Bergen, Norway.

<sup>9</sup>Geological Survey of Denmark and Greenland, Copenhagen, Denmark.

20 <sup>10</sup>Graduate School of Environmental Studies, Nagoya University, Nagoya, Japan.

<sup>11</sup>Laboratoire de Glaciologie, Université Libre de Bruxelles, Brussels, Belgium.

<sup>12</sup>School of Geography and Lincoln Centre for Water and Planetary Health, Lincoln, UK.

<sup>13</sup>Earth System Science & Departement Geografie, Vrije Universiteit Brussel, Brussels, Belgium.

<sup>14</sup>Max Planck Institute for Meteorology, Hamburg, Germany.

25 <sup>15</sup>Byrd Polar and Climate Research Center & School of Earth Sciences, The Ohio State University, Columbus OH, USA.

<sup>16</sup>Danish Meteorological Institute, Copenhagen, Denmark.

<sup>17</sup>PICE, Niels Bohr Institute, University of Copenhagen, Denmark.

<sup>18</sup>Department of Atmospheric and Oceanic Sciences, University of Colorado Boulder, Boulder CO, USA.

<sup>19</sup>Cooperative Institute for Research in the Atmosphere, Colorado State University, Fort Collins, USA.

30 <sup>20</sup>Nansen Environmental and Remote Sensing Center, Bergen, Norway.

<sup>21</sup>Department of Environmental Sciences, Western Norway University of Applied Sciences, Sogndal, Norway.

<sup>22</sup>Geophysical Institute, University of Bergen, Bergen, Norway.

<sup>23</sup>Antarctic and Sub-Antarctic Program, Universidad de Magallanes, Punta Arenas, Chile.

<sup>24</sup>Institute at Brown for Environment and Society, Brown University, USA.

35 <sup>25</sup>Department of Geography, University of Sheffield, UK.

<sup>26</sup>Lamont-Doherty Earth Observatory at Columbia University, New-York, USA.

<sup>27</sup>Department of Physical Geography, Utrecht University, Utrecht, the Netherlands.

<sup>28</sup>Department of Computer Science, University of Sheffield, UK.

<sup>29</sup>Department of Geoscience & Remote Sensing, Delft University of Technology, Delft, the Netherlands.

40 *Correspondence to:* Xavier Fettweis (xavier.fettweis@uliege.be)



**Abstract.** The Greenland Ice Sheet (GrIS) mass loss has been accelerating at a rate of about  $20 \pm 10 \text{ Gt/yr}^2$  since the end of the 1990's, with around 60% of this mass loss directly attributed to enhanced surface meltwater runoff. However, in the climate and glaciology communities, different approaches exist on how to model the different surface mass balance (SMB) components using: (1) complex physically-based climate models which are computationally expensive; (2) intermediate complexity energy balance models; (3) simple and fast positive degree day models which base their inferences on statistical principles and are computationally highly efficient. Additionally, many of these models compute the SMB components based on different spatial and temporal resolutions, with different forcing fields as well as different ice sheet topographies and extents, making inter-comparison difficult. In the GrIS SMB model intercomparison project (GrSMBMIP) we address these issues by forcing each model with the same data (i.e., the ERA-Interim reanalysis) except for two global models for which this forcing is limited to the oceanic conditions, and at the same time by interpolating all modelled results onto a common ice sheet mask at 1 km horizontal resolution for the common period 1980-2012. The SMB outputs from 13 models are then compared over the GrIS to (1) SMB estimates using a combination of gravimetric remote sensing data from GRACE and measured ice discharge, (2) ice cores, snow pits, in-situ SMB observations, and (3) remotely sensed bare ice extent from MODerate-resolution Imaging Spectroradiometer (MODIS). Our results reveal that the mean GrIS SMB of all 13 models has been positive between 1980 and 2012 with an average of  $340 \pm 112 \text{ Gt/yr}$ , but has decreased at an average rate of  $-7.3 \text{ Gt/yr}^2$  (with a significance of 96%), mainly driven by an increase of  $8.0 \text{ Gt/yr}^2$  (with a significance of 98%) in meltwater runoff. Spatially, the largest spread among models can be found around the margins of the ice sheet, highlighting the need for accurate representation of the GrIS ablation zone extent and processes driving the surface melt. In addition, a higher density of in-situ SMB observations is required, especially in the south-east accumulation zone, where the model spread can reach  $2 \text{ mWE/yr}$  due to large discrepancies in modelled snowfall accumulation. Overall, polar regional climate models (RCMs) perform the best compared to observations, in particular for simulating precipitation patterns. However, other simpler and faster models have biases of same order than RCMs with observations and remain then useful tools for long-term simulations. Finally, it is interesting to note that the ensemble mean of the 13 models produces the best estimate of the present day SMB relative to observations, suggesting that biases are not systematic among models.

## 65 1 Introduction

Mass loss from the Greenland Ice Sheet (GrIS) has been accelerating since the 1990s (Enderlin et al., 2014; Mouginit et al., 2019; Hanna et al., 2019). Over the period 1991-2015, roughly 60% of the total mass loss can be ascribed to reduced GrIS surface mass balance (SMB; see Eq. 1) (Van den Broeke, 2016), which refers to the difference between the total precipitation (rain and snow, P), runoff (RU), sublimation/evaporation (SU), snow erosion by the wind (ER) and glacier storage (GS). Since drifting snow erosion contributes  $\sim 1 \text{ Gt/yr}$  to SMB, ER is however neglected in most models, although it can be important locally (Lenaerts et al., 2012).



$$\text{SMB} = \text{P} - \text{RU} - \text{SU} - \text{ER} \quad (1)$$

75 When SMB is integrated over the whole ice sheet, the mass changes coming from the water glacial storage (lakes, melt pond, channels,...) could be relevant but has never been evaluated until now.

The recent GrIS SMB variability has been mainly driven by an increase in surface melt and subsequent meltwater runoff (Van den Broeke et al., 2016, Fettweis et al., 2017, Lenaerts et al., 2019, IPCC, 2019), caused by Arctic amplification and a  
80 state change in the North Atlantic Oscillation and increased Greenland Blocking (GBI) in summer (Fettweis et al., 2013b; Delhasse et al., 2018; Hanna et al., 2018) which raises the average temperature (Screen and Simmonds, 2010), reduces the cloudiness (Hofer et al., 2017) and enhances the melt-albedo feedback (Box et al. 2012; Ryan et al., 2019; Noël et al., 2019). Additionally, SMB-related processes are also one of the main uncertainties in future projections of the GrIS contribution to sea level rise as the ice sheet retreats in a warmer climate (Goelzer et al., 2013; van den Broeke et al., 2017; Hofer et al.,  
85 2019).

Until now, only a few attempts to compare currently available models in terms of their ability to simulate the present day GrIS SMB have been made (e.g. Vernon et al., 2013). These previous studies i) evaluated SMB within a subset of regional climate models (RCMs) (Rae et al., 2012), ii) compared positive degree day (PDD) models with energy balance snowpack  
90 models (van de Wall, 1996; Bougamont et al., 2007) or iii) assessed the representation of specific physical sub-processes (Reijmer et al., 2012). Since these models implement different physical and statistical processes, run on different grids, use different forcing data and/or cover various temporal ranges, previous model comparison studies have suffered from limited inter-comparability.

95 In this study we compare the SMB outputs of 13 state-of-the-art climate models (physical and statistical) over (1) a common time period (1980-2012), (2) using the same model grid with a 1-km horizontal resolution, and (3) over the sale ice-sheet mask of the contemporary GrIS extent. Moreover, almost all of the 13 models are forced with ERA-Interim reanalysis (Dee et al., 2011), although the data are prescribed in a slightly different manner between the models. For PDD models and energy balance models EBMs deriving melt from near-surface temperature and energy fluxes, the models are forced by the ERA-  
100 Interim based near-surface climate extrapolated to the model's spatial resolution. In Regional Climate Models (RCMs) the reanalysis dataset is prescribed at the ocean surface and at the lateral boundaries of their integration domain, while in General Circulation Models (GCMs) these forcing data are either not used or, in the case of atmosphere-only simulations, are only used to prescribe the oceanic surface conditions.

105 Sections 2 and 3 describe the 13 models used in the intercomparison (5 RCMs, 4 EBMs, 2 PDDs, and 2 GCMs) and the observational data sets used for evaluation. Results are presented in Section 4 and discussed in Section 5. Conclusions are



drawn in Section 6. Note that this intercomparison exercise does not aim at formally ranking model performance. Here we identify regions with low measurement density and large model discrepancies to provide some insight on regional uncertainty.

## 110 2. Model

### 2.1 Description

#### 2.1.1 BESSI (EBM – 10km)

BESSI is a surface energy and mass balance model designed for simulating long time scales (Born et al., 2019; Zolles et al., 2019). It is forced with ERA-interim reanalysis fields of temperature, humidity, long-wave and short-wave radiation, and  
115 precipitation (Dee et al., 2011). The temperature is the only variable that is downscaled to the actual model topography (ETOPO1, Amante and Eakins, 2009) using a lapse rate of 0.0065 K/m. Contrary to previously published model versions, here we use incoming long-wave radiation as a forcing field rather than a temperature based parameterisation. Energy fluxes are calculated with a time step of one day on a 10x10 km grid.

The model uses an albedo scheme based on a linear relationship between temperature and a time decay rate (Aoki et al.,  
120 2003). This decay is enhanced in the presence of liquid water in the surface layer. The latent and sensible turbulent heat fluxes are calculated based on the residual method (Rolstad and Oerlemans, 2005; Braithwaite, 2009) with constant wind speed over the entire ice sheet. Refreezing and percolation is instantaneous in every time step, with a maximum water holding capacity of 10% of the free pore volume (Greuell, 1992). Finally, the model parameters were optimised to fit the GRACE mass balance data over the 2002-2018 period (Born et al., 2019).

#### 125 2.1.2 BOX13 (calibrated RCM – 5km)

The basis of the BOX13 surface mass balance reconstruction are linear regression parameters that describe relationships between spatially discontinuous in-situ records from meteorological stations (i.e. monthly temperature after Vinther et al. (2006); Cappelen et al. (2001, 2006, 2011) or firn/ice cores and spatially continuous RACMO2.1 (Ettema et al., 2010) regional climate model output. Explanatory (independent variable) data (air temperature and firn/ice core data) span 1840 to  
130 2012. A 43-year overlap period 1960-2012 with RACMO2.1 is used to determine regression parameters on a grid cell basis. A fundamental assumption is that the calibration factors; regression slope and offset for the calibration period 1960-2012; is stationary in time.

The RACMO2.1 data are resampled and reprojected from a 0.1 deg (~10 km) grid to a 5 km grid. See Box et al. (2013) 'part  
135 I' for a description of the method, that includes a formal approach to estimate uncertainty. The following refinements are however made from the SMB reconstruction of Box et al. (2013) and Box (2013). The estimation of values is made for a



domain that includes not only ice but land and sea. The physically-based meltwater retention scheme of Pfeffer et al. (1991) replaced the simpler approach used by Box (2013). Multiple station records contribute to the near surface air temperature for each given year, month and grid cell in the domain while in Box (2013), only data from the single highest correlating station yielded the reconstructed value. This revised surface mass balance data ends with year 2012 while Box (2013) ends in 2010. Finally, the annual accumulation rates from ice cores are dispersed into a monthly temporal resolution by weighting the monthly (based on the 1960-2012 RACMO2.1 data) fraction of the annual total for each grid cell in the domain. The accumulation reconstruction has been evaluated by Lewis et al. (2017, 2019).

### 2.1.3 CESM2 (GCM – 1km)

In this study, the CESM version 2.0 (CESM2) is used in a configuration with fixed ocean state. In particular, the protocol for the Atmospheric Model Intercomparison Project (AMIP, Gates et al., 1999) is used, with prescribed sea-surface temperatures and sea ice cover from Hurrell et al. (2008) for the period 1979-2014. Global land cover usage is prescribed. The atmospheric component is the Community Atmosphere Model version 6 (CAM6) and the land surface component is the Community Land Model version 5 (CLM5), both operating at a nominal resolution of 1 degree. No ice dynamics are considered, i.e. the geometry of the GrIS is static in time. Initial conditions for CAM6 and CLM5 snow pack are taken from a fully coupled CESM2 simulation. Subgrid topographic variability is partially accounted for by the use of multiple elevation classes (ECs) in CLM5, with up to 10 ECs per grid cell. Atmospheric forcing is downscaled to each EC, with lapse rates used for temperature and downwelling longwave radiation, and phase recomputation for precipitation (for details: see Van Kampenhout et al., 2019). Output indexed by EC is used for downscaling CESM2 SMB to the 1 km ISMIP6 grid (Nowiki et al., 2016) using linear interpolation in the vertical and bilinear interpolation in the horizontal direction as described in Van Kampenhout et al. (2019).

### 2.1.4 dEBM (EBM – 1km)

The diurnal Energy Balance Model (dEBM) is a surface mass balance scheme that incorporates both radiative and turbulent heat fluxes, and captures diurnal variability in the melt-freeze cycles (Krebs-Kanzow et al., 2018) and monthly variations in cloud cover. As forcing, dEBM only requires monthly means of short wave radiation at the surface, near surface air temperature and precipitation. Monthly mean duration and intensity of the diurnal melting and refreezing periods are derived from the monthly mean surface radiation and from the diurnal cycle of the top of atmosphere (TOA) short wave radiation. The latter is implicitly represented as a function of latitude and month based on prescribed parameters of the Earth's orbit around the Sun. Monthly mean atmospheric transmissivity and cloud cover are estimated from the ratio between monthly mean shortwave radiation at the surface and at the TOA (from forcing fields and from orbital parameters, respectively). The scheme has a monthly time step and distinguishes albedo of bare ice, and wet, dry and new snow on the basis of precipitation, surface energy balance and the previous month's snow type and snow height. Additionally, the scheme includes a residual heat flux  $R$  which is thought to represent those energy fluxes which are not included in the scheme, such



as the heat flux to the subsurface or latent heat fluxes at the surface. Here,  $R$  has been treated as a tuning parameter and has  
170 been optimized to  $R = -5\text{W m}^{-2}$  with respect to the surface mass balance measurements from Machguth et al. (2016) over the  
ERA-Interim period (1979-2016). To force the model, monthly mean ERA-Interim precipitation, surface insolation and near  
surface air temperatures have been interpolated to the 1 km ISMIP6 grid and temperature fields have been additionally  
downscaled applying a lapse rate correction of  $\Gamma = -0.007\text{K/m}$ .

#### 2.1.4 HIRHAM (RCM – 5.5km)

175 The HIRHAM regional climate model has been developed to include a full surface energy and mass balance model using an  
original code developed from physical schemes used in the ECHAM5 global model and dynamical schemes from the  
HIRLAM numerical weather prediction model. It has 31 vertical levels and is forced on 6 hourly intervals on the lateral  
boundaries. The RCM has a simple five layer snowpack model to a depth of 10m over glacier surfaces, incorporating the  
same parameterisations used in an offline version that has 32 layers. The offline version assimilates MODIS MOD10A  
180 albedo data to get a closer fit between modelled and observed albedos. Langen et al. (2017) describe the snowpack model in  
detail and show that the inclusion of MODIS data significantly improves the modelled SMB.

#### 2.1.6 IMAU-ITM (EBM – 5km)

IMAU-ITM is an insolation- and temperature-based SMB model. This simplified EBM is used in the ANICE ice-sheet  
model for paleoclimate simulations (de Boer et al., 2014; Berends et al., 2018). Monthly precipitation from the ERA-Interim  
185 reanalysis is downscaled to actual model topography (in this case, the BedMachine v3 dataset; Morlighem et al., 2017) using  
the wind-orography-based parameterisation by Roe and Lindzen (2001) and Roe (2002). The resulting downscaled  
precipitation is partitioned into rain and snow based on the temperature parameterisation by Ohmura (1999). The depth of  
the accumulated snow layer is tracked, with a maximum value of 10 m; any additional firm is assumed to be compressed into  
ice. The surface albedo is calculated as a weighted average of the albedos of fresh snow and bare ice, based on the thickness  
190 of the snow layer and the amount of melt that occurred during the previous year. Melt is determined using the insolation-  
temperature parameterisation by Bintanja et al. (2002), which uses prescribed values for insolation at the top of the  
atmosphere, and which was developed especially for palaeoglaciological applications. Refreezing is calculated following the  
approach by Huybrechts and de Wolde (1999) and Janssens and Huybrechts (2000), based on the available liquid water (the  
sum of rain and melt) and the refreezing potential, integrated over the entire year to account for the retention of summer melt  
195 which is refrozen in winter. For this study, the parameters in the refreezing and snowmelt parameterisations were calibrated  
to obtain the closest match (i.e. highest value of linear correlation coefficient divided by RMSE) to the RACMO2.3 values  
over the 1979-2017 period on the 1 km grid.



### 2.1.7 MAR (RCM - 15km)

The version 3.9.6 from MAR is used here by using a resolution of 15 km. MAR was forced at its lateral boundaries by ERA-  
200 Interim at a 6-hourly time step. The boundary forcing files include information about the temperature, u- and v- wind  
components, specific humidity and sea level pressure as well as the sea surface temperature (SST) and sea ice cover over  
ocean. It is the same model configuration which is used in the Ice Sheet Model Intercomparison Project for CMIP6 (ISMIP6)  
for future projections over the GrIS (Nowiki et al., 2016). With respect to the version 3.5.2 of MAR used in Fettweis et al.  
(2017) and Hofer et al. (2017), the main improvements are: (1) An increase of the cloud lifetime with the aim of correcting  
205 the biases of solar and infrared radiation highlighted in Fettweis et al. (2017), (2) adjustments in the bare ice albedo  
representation for a better comparison with in situ measurements, (3) a larger independence of model results to the used time  
step and (4) a better dynamical stability with an increased spatial filtering for a computing time divided by a factor 2  
compared to version 3.5.2. Additionally, we also dealt with minor bug corrections and small updates for enhanced  
computing efficiency and comparison with in-situ automatic weather data (Delhasse et al., 2019).

### 210 2.1.8 MPI-ESM (GCM - 1km)

The historical simulation underlying the SMB calculations by Max Planck Institute (MPI) is simulated with a higher  
resolution version of the latest version of the MPI Earth System Model (MPI-ESM1.2-HR). In this version the atmospheric  
model ECHAM6.3, with a spectral resolution of T127 (~100 km), is coupled to the ocean model MPIOM version 1.6.2, with  
a nominal 0.4° resolution and a tripolar grid. A thorough description of this model setup can be found in Müller et al. (2018).  
215 An EBM approach is used to calculate the SMB from one ensemble member of the historical MPI-ESM1.2-HR simulations  
and downscale it from ~100km to the 1km ISMIP6 topography. The offline EBM scheme is similar to the one presented in  
Vizcaino et al. (2010); despite technical changes and the introduction of elevation classes mainly the albedo parameterisation  
was updated. The EBM calculates melt and accumulation rates from hourly atmospheric fields of the historical MPI-  
ESM1.2-HR simulation on its native grid. The atmospheric fields are bi-linearly interpolated onto 24 fixed elevation classes,  
220 ranging from 0 m to 8000 m. To account for height differences between each elevation class and the surface elevation of the  
atmospheric model a height correction is applied to near-surface air temperature, humidity, dew point temperature,  
precipitation, downward longwave radiation and near-surface density fields. The downward shortwave radiation is kept  
constant, as it is largely affected by atmospheric properties that are independent of elevation differences (e.g. ozone  
concentration, aerosol thickness) (Yang et al., 2006). To obtain melt rates, the EBM computes the energy balance at the  
225 atmosphere-snow interface as sum over the radiative and turbulent as well as rain induced and conductive heat fluxes. The  
albedo parameterisation used here is based on the parameterisation by Oerlemans and Knap (1998) and considers snow  
aging, snow depth, and the influence of cloud coverage. The obtained 3-D fields of surface melt, accumulation and SMB are  
then vertically and horizontally interpolated onto the 1km ISMIP6 topography used as reference topography in this study.



### 2.1.9 NHM-SMAP (RCM – 5km)

230 The latest version of the polar RCM NHM-SMAP, with a horizontal resolution of 5 km, developed by Niwano et al. (2018) was used in this study. The same version was recently utilised to assess cloud radiative effects on the Greenland ice sheet surface melt (Niwano et al., 2019). The atmospheric part of NHM-SMAP is the Japan Meteorological Agency Non-Hydrostatic atmospheric Model (JMA-NHM) developed by Saito et al. (2006), which employs flux form equations in spherical curvilinear orthogonal coordinates as the governing basic equations. We pay close attention to the cloud  
235 microphysics processes, therefore, the version of JMA-NHM utilised for NHM-SMAP (Hashimoto et al., 2017) employs a double-moment bulk cloud microphysics scheme to predict both the mixing ratio and the concentration of solid hydrometeors (cloud ice, snow, and graupel), and a single-moment scheme to predict the mixing ratio of liquid hydrometeors (cloud water and rain). For the simulation of snow and ice physical conditions, the multilayered physical snowpack model SMAP is utilised (Niwano et al., 2012, 2014). The SMAP model calculates snow albedo using the detailed physically based  
240 snow albedo model developed by Aoki et al. (2011) considering the effects of snow grain size evolution explicitly. Although the model can also consider the effects of light-absorbing impurities on snow albedo, we assumed the pure snow condition here. On the other hand, bare ice albedo is calculated by using a simple parameterisation as a function of density. To estimate realistic runoff from the ice sheet, a detailed vertical water movement scheme based on the Richards equation (Yamaguchi et al., 2012) is used. To force NHM-SMAP (dynamical downscaling), we used not the ERA-Interim reanalysis but the JRA-55  
245 reanalysis (Kobayashi et al., 2015) due to the lack of enough computational resources. However, it should be noted that the quality of the arctic atmospheric physical conditions from both reanalysis data during the study period were almost the same level as reported by Simmons and Poli (2015) and Fettweis et al. (2017) who showed not significant difference between MAR forced by ERA-Interim and JRA-55.

### 2.1.10 PDD5km (PDD - 5km)

250 European Centre for Medium-Range Weather Forecasts (ECMWF) ERA-Interim (Dee et al., 2011) 2-m surface air temperature, precipitation and surface latent heat flux reanalysis data were downscaled from their native 0.75° resolution to 5x5-km using bilinear interpolation, a high-resolution DEM (Ekholm, 1996) and empirically-derived ice-sheet surface lapse rates to correct surface air temperature, as described in full in Hanna et al. (2005, 2011). Downscaled surface air temperature was validated using independent in-situ observational automatic weather station data from the Greenland Climate Network  
255 (Steffen and Box, 2001), showing very good agreement between downscaled/modelled and observed temperatures. Net solid precipitation (snowfall minus evaporation and sublimation) was spatially calibrated against the Bales et al. (2009) krigged map of snow accumulation based on ice-core and coastal precipitation gauges. Evaporation and sublimation were calculated from surface latent heat flux. The resulting downscaled Greenland climate gridded data were used to drive a runoff/retention model (Janssens and Huybrechts, 2000) that produced surface melt, runoff, evaporation and SMB at a monthly time  
260 resolution, while net precipitation was taken from the ERA-I dataset downscaled, calibrated and adjusted as above. Ice-sheet



averaged annual SMB since 1958 was shown to correlate strongly between this method and RACMO2.1 but significant differences in absolute values between the respective methods were considered to be mainly due to poorly-constrained modelled accumulation (Hanna et al., 2011).

### 2.1.11 PDD1km (PDD - 1km)

265 This modelling method is essentially the same as described in 2.1.10. However, here a higher-resolution DEM (Bamber et al., 2013) was used to downscale ERA-Interim reanalysis data to 1x1 km<sup>2</sup> resolution, producing monthly output for 1979-2012 (Wilton et al., 2017). In addition, variable “sigma” - standard deviation of 6-hourly temperatures, computed for each month- was incorporated into the PDD method, based on earlier work by Jowett et al. (2015). The resulting high-resolution PDD model output was evaluated using PROMICE observations (Machguth et al., 2016), showing generally robust  
270 correlations (Wilton et al., 2017) which were broadly comparable, though not quite as good, as the polar RCMs. Finally, this method is particularly useful for long centennial/pre-satellite timescales for which relatively few reliable meteorological fields are available (Wilton et al., 2017).

### 2.1.12 RACMO2.3 (RCM - 1km)

The polar (p) version of the Regional Atmospheric Climate Model (RACMO2.3p2) is run at 5.5 km horizontal resolution for  
275 the period 1958-2018 (Noël et al., 2018). The model incorporates the dynamical core of the High-Resolution Limited Area Model (HIRLAM; Undèn et al., 2002) and the physics from the European Centre for Medium-range Weather Forecasts-Integrated Forecast System (ECMWF-IFS cycle CY33r1; ECMWF-IFS, 2008). RACMO2.3p2 includes a multi-layer snow module that simulates melt, water percolation and retention in snow, refreezing and runoff (Ettema et al., 2010). The model also accounts for dry snow densification (Ligtenberg et al., 2018), and drifting snow erosion and sublimation (Lenaerts et al.,  
280 2012). Snow albedo is calculated based on snow grain size, cloud optical thickness, solar zenith angle and impurity concentration in snow (Van Angelen et al., 2012). Bare ice albedo is prescribed from the 500 m MODIS 16-day Albedo product (MCD43A3), as the 5% lowest surface albedo records for the period 2000-2015, minimized at 0.30 for dark bare ice and maximized at 0.55 for bright ice under perennial firn. Glacier outlines and surface topography are prescribed from a down-sampled version of the 90 m Greenland Ice Mapping Project (GIMP) Digital Elevation Model (DEM) (Howat et al.,  
285 2014). RACMO2.3p2 is forced at its lateral boundaries by ERA-40 (1958-1978) (Uppala et al., 2005) and ERA-Interim (1979-2018) (Dee et al., 2011) re-analyses on a 6-hourly basis within a 24 grid cells wide relaxation zone. The forcing consists of temperature, specific humidity, pressure, wind speed and direction being prescribed at each of the 40 vertical atmosphere model levels. Upper atmosphere relaxation (nudging) is also implemented in RACMO2.3p2 (Van de Berg and Medley, 2016). The model has 40 active snow layers that are initialized in September 1957 using temperature and density  
290 profiles derived from the offline IMAU Firn Densification Model (IMAU-FDM) (Ligtenberg et al., 2018). Detailed description of the model and recent updates are discussed in Noël et al. (2018).



The 5.5 km product is further statistically downscaled onto a 1 km grid to resolve the steep SMB gradients over narrow glaciers and confined ablation zones at the rugged ice sheet margins. Statistical downscaling corrects runoff for biases in elevation and bare ice albedo using a down-sampled version of the GIMP DEM (topography and ice mask) and a MODIS  
295 albedo product at 1 km resolution. This allows to accurately represent the high runoff rates observed at the GrIS margins, significantly improving the agreement with SMB measurements. Detailed description of the statistical downscaling procedure is discussed in Noël et al. (2016).

### 2.1.13 SnowModel (EBM - 5km)

SnowModel was forced with ERA-Interim (ERA-I) reanalysis products on a  $0.75^\circ$  longitude  $\times$   $0.75^\circ$  latitude grid from the  
300 European Centre for Medium-Range Weather Forecasts (ECMWF; Dee et al. 2011), where the 6-hour (precipitation at 12-hour) temporal resolution ERA-I data were downscaled to 3-hourly values and a 5-km grid. SnowModel (Liston and Elder, 2006a) contains six sub-models, where five of the models were used here to quantify spatiotemporal variations in atmospheric forcing, GrIS surface snow properties (including refreezing and retention), sublimation, evaporation, runoff, and SMB. The sub-model MicroMet (Liston and Elder, 2006b; Mernild et al., 2006) downscaled and distributed the  
305 spatiotemporal atmospheric fields using the Barnes objective interpolation scheme, where the interpolated fields were also adjusted using known meteorological algorithms, e.g., temperature-elevation, wind-topography, humidity-cloudiness, and radiation-cloud-topography relationships (Liston and Elder, 2006b). Enbal (Liston, 1995; Liston et al., 1999) simulated a full surface energy balance considering the influence of cloud cover, sun angle, topographic slope, and aspect on incoming solar radiation, and moisture exchanges, e.g., multilayer heat- and mass-transfer processes within the snow (Liston and Mernild,  
310 2012). SnowTran-3D (Liston and Sturm, 1998, 2002; Liston et al., 2007) accounted for the snow (re)distribution by wind. SnowPack-ML (Liston and Mernild, 2012) simulated multilayer snow depths, temperatures, and water-equivalent evolutions. HydroFlow (Liston and Mernild, 2012) simulated watershed divides, routing network, flow residence-time, and runoff routing (configurations based on the hypothetical gridded topography and ocean-mask datasets), and discharge hydrographs for each grid cell including from catchment outlets. These sub-models have been tested against independent observations  
315 with success in Greenland, Arctic, high mountain regions, and on the Antarctic Ice Sheet with acceptable results (e.g., Liston and Hiemstra, 2011; Mernild and Liston, 2012; Mernild et al., 2015; Beamer et al., 2016).

### 2.2 Interpolation on a common grid

One of the key issues raised by the first SMB model intercomparison performed by Vernon et al. (2013) was the high dependency of modelled integrated SMB values to the used ice sheet mask. To mitigate this problem, we extrapolated all  
320 model outputs to the same 1-km grid used in the Ice Sheet Model Intercomparison Project for CMIP6 (ISMIP6). This resolution was chosen because the highest resolution model outputs (e.g. RACMO2.3p2) are available at 1 km and choosing a coarser resolution could compromise their quality. A common grid also allowed comparison on two common ice sheet masks: the contiguous Greenland ice sheet, which is common to all the models and the Greenland ice sheet plus peripheral



ice caps and mountain glaciers, common to all the models except the two PDD models. Unless otherwise indicated, the SMB  
325 components have been interpolated to 1 km using a simple linear interpolation metric of the four nearest inverse-distance-  
weighted model grid cells. Moreover, as done in Le Clech't et al. (2019), the interpolated 1km SMB and runoff fields have  
been corrected for elevation differences between the model native topography and the GIMP 250 m topography (interpolated  
to 1 km here), using a time and space varying SMB-elevation gradients, as described in Franco et al. (2012) and in Noël et  
al. (2016). No correction was applied to precipitation after interpolation to 1km. Finally, the ensemble mean is based on the  
330 average of the 13 modelled monthly outputs interpolated on the 1km grid.

### 3. Observational data

#### 3.1. Ice core and SMB measurements.

Similar to Fettweis et al. (2017), we compare modelled SMB with in-situ observations from:

(1) ice core measurements in the accumulation zone (Bales et al., 2001, 2009; Ohmura et al., 1999). The model outputs are  
335 averaged over the overlapping measurements period. We use the annual mean over 1980-2012 when the measurements  
period is not specified or outside the period 1980-2012. This allows to extend a bit the amount of available ice core  
measurements for model evaluation without changing in deep the statistics. The modelled SMB values are compared to ice  
cores by interpolating the four nearest inverse-distance-weighted grid cells to the common 1-km ISMIP6 grid.

340 (2) the SMB database (Machguth et al., 2016) compiled under the auspice of PROMICE and available through the  
PROMICE web portal (<http://www.promice.dk>). This dataset mainly covers the ablation zone of the GrIS and includes  
measurements over some peripheral ice caps (as shown in Fig 1). Measurements not included in 1980-2012 period, records  
shorter than 3 months or located outside the common 1 km ice mask are discarded from the comparison. In a similar fashion  
as in Wilton et al. (2017), monthly model outputs are weighted by the length of the observed month, e.g. if the record starts  
345 in the middle of a month. Daily outputs, available for some models, are not used here. As for the ice cores, outputs are  
interpolated using the four nearest inverse-distance-weighted grid cells onto the ISMIP6 ice mask.

(3) the unpublished database of snow pits (Jason Box, personal communication) incorporating observations of winter  
accumulation over previously exposed bare ice or firn. Snow pits were monitored at the end of the following winter  
350 accumulation period (usually in May). As only the date when the snow pits were dug is known (May), we assume, for the  
comparison with the models, that each record has started on the 1st of September. However, for some years and locations,  
the winter accumulation may have started slightly later in October or November, after some late-season melt events. That is  
why, we have accumulated modelled SMB values from September to May when the monthly modelled SMB is positive.



### 3.2. GRACE estimation

355 The GRACE-based product, coupled with an estimate of monthly ice discharge from all ( $n > 200$ ) large outlet glaciers (King et al., 2018), is used here to evaluate the trend of the 2003-2012 modelled SMB. These quantities are integrated over the 6 basins defined in King et al. (2018) and based on basin configurations from Sasgen et al. (2012). The correction for glacial isostatic adjustment is based on the model of Khan et al., 2016. Monthly glacier discharge estimates are combined with RACMO2.3p2 SMB, and compared the resulting mass balance estimate to the GRACE product. It is important to note that  
360 these discharge/GRACE products from King et al. (2018) were derived independently from RACMO3.2p2, and can therefore be used to evaluate the trends in SMB products.

### 3.3. Bare ice extent

The MODIS-based bare ice monthly product was used to evaluate the mean extent of the ablation zone (i.e. where the mean annual SMB is negative) simulated by the models over 2000-2012 (Ryan et al., 2019). The daily classified bare ice maps  
365 were used to calculate a summer (June, July, and August) bare ice presence index (or exposure frequency). The bare ice presence index varies between 0 and 1 in any given summer and is defined as the number of times a pixel is classified as bare ice divided by the total number of valid observations of that pixel (i.e., when not cloud obscured) between June 1 and August 31. Finally, a  $1 \times 1$  km<sup>2</sup> pixel was considered within the ablation zone if it was detected as bare ice in at least 50% of the summers in 2000-2012.

## 370 4. Evaluation of models

### 4.1 Comparison with in-situ SMB measurements

In comparison with SMB derived from ice cores (location shown in Fig. 1), both PDD models perform the best (See Table 1). However, the same ice core dataset has been used to correct ERA-interim precipitation that is used to force both these models, therefore they are not completely independent. Furthermore, the RCMs MAR, NHM-SMAP and RACMO2.3  
375 generally agree better with observations than the other models that use ERA-Interim precipitation as forcing or GCM-based precipitation computed at lower spatial resolution. Except for the two PDD models, the RMSE of the models is generally higher than the standard deviation of the ice core measurements.

All the models show a worse agreement with the 130 snow pits than with the ice cores measurements (Table 1). However a  
380 large part of these discrepancies can likely be ascribed to the use of monthly outputs knowing that the starting date of the snow pit records (i.e. when the winter accumulation actually started) is uncertain. With respect to the PROMICE SMB data set, the model RMSE varies between 0.48 mWE (for MAR) and 0.89 mWE (for BESSI) over the main ice sheet. For most of the models, the RMSE is close to the temporal standard deviation (0.92 mWE) of the PROMICE data set, suggesting that the



385 modelled biases are not statistically significant. Finally, it is interesting to note that the best statistics are performed with the ensemble mean of the 13 models (see Fig. S1 in supplementary), which will be used hereafter as the SMB reference field. This suggests also that biases of each model are of different signs and are compensated when the 13 models based estimates are averaged.

390 All models, except HIRHAM, underestimate accumulation above 0.5 mWE but underestimate ablation rates when they are greater than 3 mWE, except RACMO2.3 and the two PDD models. Between 0 and 2 mWE, most of the models rather overestimate ablation (Fig. 1). Finally, BESSI, BOX13 and NHM-SMAP systematically underestimate the ablation rates over the whole range of observations, explaining their unfavourable statistics in Tab. 1 relative to other models.

In brief, it is interesting to note that all types of model generally show similar performance (see Fig. S1 in supplementary). 395 Computationally expensive models (i.e. the RCMs) give the best agreement with observations: MAR and RACMO2.3 perform well on average compared to SMB observations GrIS-wide, while NHM-SMAP (resp. HIRHAM) performs better at representing SMB in the accumulation zone (resp. in the ablation zone). However, the evaluation statistics from the more simple models (PDDs and EBMs) and from GCMs are generally similar to the ones of polar RCMs. It is nevertheless important to note that RCMs are often used to calibrate these models, partly explaining their general good performance.

#### 400 **4.2 Comparison with GRACE measurements**

To enable comparison with GRACE mass change, we estimate total mass balance (MB) for each model in 6 basins (Fig. 3) by subtracting observed ice discharge (King et al., 2018) from modelled SMB for the 13 models. Over Basin 1 and 2, IMAU-ITM and SnowModel (resp. CESM2 and MPI-ESM) overestimate (resp. underestimate) GRACE mass loss over 2003-2012. Over Basin 3, all the models underestimate the mass change. Additionally, some of the models (in particular 405 MAR) do not simulate mass variations in Basin 3, despite GRACE data suggesting a mass loss of 450 Gt over 2003-2012. In south Greenland (Basin 4), the two PDD models show the most favourable statistics but all the models (except MPI-ESM) underestimate mass loss. Along the west coast (Basin 5 and Basin 6), MAR and RACMO2.3 are most closely aligned with the observations, while SnowModel systematically overestimates, and NHM-SMAP systematically underestimates the mass loss. For the other models, the bias in Basin 5 and 6 varies in sign. Finally, an EBM (dEBM), a GCM (MPI-ESM), a PDD 410 (PDD1km) and two RCMs (MAR and RACMO2.3) compare the closest to the GRACE based GrIS-integrated mass loss over 2003-2012. These favourable statistics are due to error compensation as none of the models matches well the GRACE-derived regional mass loss integrated over individual basins. However, we need to mention that all of our modelled total mass balance estimations use the same discharge estimates from King et al. (2018) and do not take into account changes in mass over tundra, over small ice caps (not included in the common ice sheet mask) and in glacial storages (e.g. meltwater 415 lakes, water tables,...): this partly explains why the discrepancies between models and GRACE could be locally very high.



420 Additionally, the statistics listed in Table 2 are useful for evaluating the seasonal variability once the linear trend in both time series has been removed. In comparison to GRACE we find that the five RCMs simulate the seasonal cycle of SMB much better than other types of models (see Fig. S2 in supplementary), although the trend (Fig. 3) is significantly underestimated in e.g. HIRHAM and NHM-SMAP. The two GCMs have the larger RMSE mainly because their interannual variability is not (fully) forced by ERA-Interim. Finally, it is interesting to note that, for most of the models, the sign of the bias with the PROMICE data set (see Table 1) is highly correlated to the sign of the trend bias with respect to the GRACE based product. For example, the 2003-2012 changes in SMB were driven by an increase of melt, and those models underestimating surface ablation also underestimate these recent changes (the signal coming from discharge change is the same for all the models). Finally, for a total surface mass loss over 2003-2012 of  $\sim 3000$  Gt as suggested by the GRACE data set, the models range from -1066 Gt to -6034 Gt with an ensemble mean of  $-2611 \pm 1253$  Gt suggesting a large discrepancy between models and therefore a large uncertainty in the modelled SMB trends.

#### 4.3 Comparison with bare ice extent

430 We can reasonably assume that the mean SMB should be negative in the bare ice area and positive above the snow line. However, the equilibrium line altitude varies each year. Therefore, we have chosen to only use SMB values that fall within 0 mmWE/yr plus (resp. minus) half the SMB interannual variability ( $/2$ ) to detect the modelled accumulation (resp. ablation) zone. Except BESSI, all models are able to develop a large enough bare ice area, although most of them overestimate the ablation zone extent, in particular IMAU-ITM and SnowModel (see Table 3). In Fig. 2, the hatched areas outline the regions where the models overestimate or underestimate (only for BESSI) the bare ice area. We can see that BESSI fails to represent the extent of the south-western ablation zone. Conversely, IMAU-ITM, BOX13, PDD5km and SnowModel overestimate the extent of the ablation area in north-east Greenland, where the SMB from the other models is also very low but remains positive. Finally, it is interesting to note that both GCMs (CESM2 and MPI-ESM), despite their coarse native resolution in the atmosphere, are able to accurately model the snow line, which is attributed to their subgrid downscaling module.

#### 5. Discussion and comparison

440 Integrated over the common main ice sheet mask (see Table 4), the average total GrIS SMB over 1980-2012 ranges from 96 Gt/yr (SnowModel) to 429 Gt/yr (NHM-SMAP), with a mean value of  $340 \pm 112$  Gt/yr. Comparing the two largest SMB components (i.e. snowfall and runoff), we show large discrepancies between models. For some models, SMB falls within the range of the other models only due to compensating effects of over or underestimating both snowfall and runoff (see Fig. S3 in supplementary). For example, the snowfall and runoff from BESSI and the PDD models are very low compared to other models but yield similar integrated SMB. In addition, the SMB of NHM-SMAP (resp. SnowModel) is substantially higher (resp. lower) than that of other models, due to an overestimation in snowfall accumulation (resp. meltwater runoff). Finally,



except for SnowModel (which suggests an SMB trend close  $-12.9 \text{ Gt/yr}^2$ ), all models suggest that the SMB of the GrIS has decreased at a rate of  $\sim 7 \text{ Gt/yr}^2$  over the period 1980-2012, primarily due to an increase of meltwater runoff ( $\sim +8 \text{ Gt/yr}^2$ ).

450 If we compare each model to the ensemble mean (Fig. 4), we can see that BESSI, NHM-SMAP and PDD1km generally simulate lower runoff in the ablation zone with respect to the other models (Fig. 5). In contrast SnowModel, HIRHAM and BOX13 simulate rather larger runoff than the ensemble mean. These differences mainly explain the SMB anomaly in the ablation zone shown in Fig 4 with respect to the ensemble mean. IMAU-ITM, BESSI and SnowModel are too dry in the interior of the ice sheet, even though they use identical ERA-Interim precipitation forcing as the other PDD/EBM models  
455 (Fig. 6). In the accumulation zone of south Greenland, CESM overestimates snowfall rates while MPI-ESM underestimates them in addition of overestimating runoff in this area. Finally, for all the RCMs, the snowfall accumulation does not show similar and systematic anomalies over a large extent and oscillates around the ensemble mean. This a priori better representation of precipitation spatial variability in the RCMs is likely due to the fact that the precipitation is computed at higher resolution than in the GCMs or in ERA-Interim reanalysis used to force the PDD/EBM models. This highlights the  
460 advantage of simulating precipitation at high spatial resolution in order to represent the interaction between the atmospheric flow and ice-sheet topography. The south-east coast of Greenland shows the largest discrepancy between models, reaching  $2 \text{ mWE/yr}$  locally, and is where most RCMs simulate higher precipitation than other types of models. Unfortunately, the data coverage along the south-eastern coast is very sparse, making it hard to prove whether high accumulation rates in RCMs, locally exceeding  $3 \text{ mWE/yr}$ , are actually realistic. This highlights the need for a higher density of in situ measurements in  
465 southeast Greenland where the models simulate the maximum of precipitation. Shallow ice radar or remote sensing (elevation satellite) could also help to evaluate the accumulation rates in this area.

## 6. Conclusion

This paper describes the methodology and results of the SMB Model Intercomparison Project (GrSMBMIP): a novel effort that intercompares GrIS SMB fields produced using 5 RCMs, 4 EBMs, 2 PDDs, and 2 GCMs. Model evaluation using ice  
470 core data highlights that polar RCMs (in particular MAR and RACMO2.3) have the most accurate representation of SMB in both the GrIS accumulation and ablation zones but they are also the only ones to have been calibrated to simulate separately snowfall and melt which not all models do. Biases of other models are nevertheless on the same order to those of polar RCMs (which are often used to calibrate these more simple but faster models) and the ensemble mean of the 13 inter-compared models compares best with the SMB in situ observations. The good performance of the PDD models in the  
475 ablation zone suggests that estimating melt from temperature remains valid under current climate conditions and that the use of more sophisticated energy balance melt scheme (like the ones used in SnowModel and NHM-SMAP) can generate larger biases than resolving them with a priori better physics. Finally, the mean bias in the ablation zone mostly explains the large discrepancy between models and GRACE-derived mass loss trend in 2003-2012. This suggests that biases over current



climate could strongly impact the models' ability to simulate future meltwater runoff acceleration and associated sea level  
480 rise (Fettweis et al., 2013a).

RCMs have the advantage that they resolve near-surface climate and dynamically downscale the precipitation to higher  
spatial resolution with respect to their forcing whereas the PDD and EBM models are fully driven by the near-surface  
climate of their low resolution forcing fields. While the two GCMs used in this study are not (or not fully) forced by ERA-  
485 Interim, they reasonably simulate the melt, that can likely be ascribed to subgrid elevation corrections applied in MPI-ESM  
and CESM2. However, for precipitation, the native GCM resolution remains too coarse to resolve the spatial variability  
simulated by RCMs. The spatial variability of precipitation in RCMs is particularly high along the southeast coast of  
Greenland. However, the paucity of observations prevents us from confirming whether the local high precipitation rates  
simulated by RCMs and not captured by lower resolution models are realistic. Moreover, running RCMs at a high spatial  
490 resolution becomes computationally expensive on time scales beyond one century suggesting that the PDD/EBM and GCM  
based approaches may be more suitable for questions that require long simulations (where a coupling to an ice sheet model  
may be desirable as well).

The different types of models show large discrepancies in regional mass loss trends with respect to GRACE estimates (2003-  
495 2012) in the trend of surface mass loss between the models compared here. Comparing outputs from these same models in a  
future warmer climate will enable an improved quantification of uncertainties in climate projections and therefore help refine  
estimates of the GrIS contribution to future sea level rise.

*Data availability.* All the modelled data sets presented in this study are available from the authors upon request and without  
500 conditions.

*Author contributions.* XF and SH prepared the manuscript. UKK provides figures in Supplementary. All authors commented  
and improved the manuscript.

505 *Competing interests.* The authors declare no competing interests.

*Acknowledgements.* Xavier Fettweis is a Research Associate from the Fonds de la Recherche Scientifique de Belgique  
(F.R.S.-FNRS). Computational resources used to perform MAR simulations have been provided by the Consortium des  
Équipements de Calcul Intensif (CÉCI), funded by the Fonds de la Recherche Scientifique de Belgique (F.R.S.FNRS) under  
510 grant 2.5020.11 and the Tier-1 supercomputer (Zenobe) of the Fédération Wallonie Bruxelles infrastructure funded by the  
Walloon Region under grant agreement 1117545. Andreas Born and Tobias Zolles acknowledge financial support from the  
Trond Mohn Foundation. Constantijn J. Berends and Heiko Goelzer have received funding from the programme of the



Netherlands Earth System Science Centre (NESSC), financially supported by the Dutch Ministry of Education, Culture and Science (OCW) under grant no. 024.002.001. Edward Hanna acknowledges support from the University of Sheffield's  
515 Iceberg high-performance computing team, especially Mike Griffiths. Philippe Huybrechts acknowledges support from the iceMOD project funded by the Research Foundation – Flanders (FWO-Vlaanderen). Marie-Luise Kapsch and Florian Ziemen were funded by the German Federal Ministry of Education and Research (BMBF) through the PalMod project under grant no. 01LP1504C and 01LP1502A. Bert Wouters was funded by NWO VIDI grant 016.Vidi.171.063.

## References

- 520 Amante, C. and Eakins, B.: ETOPO1 1 Arc-Minute Global Relief Model: Procedures, Data Sources and Analysis, <https://doi.org/doi:10.7289/V5C8276M>, 2009.
- Aoki, T., Hachikubo, A., and Mashiro, H.: Effects of snow physical parameters on shortwave broadband albedos, *Journal of Geophysical Research*, 108, 1–12, <https://doi.org/10.1029/2003JD003506>, 2003.
- Aoki, T., Kuchiki, K., Niwano, M., Kodama, Y., Hosaka, M., and Tanaka, T.: Physically based snow albedo model for  
525 calculating broadband albedos and the solar heating profile in snowpack for general circulation models, *J. Geophys. Res.*, 116, D11114, <https://doi.org/10.1029/2010JD015507>, 2011.
- Bales, R.C., Q. Guo, D. Shen, J.R. McConnell, G. Du, J.F. Burkhart, V.B. Spikes, E. Hanna, J. Cappelen: Annual accumulation for Greenland updated using ice core data developed during 2000-2006 and analysis of daily coastal meteorological data. *J. Geophys. Res.* 114, D06116, 2009.
- 530 Bamber, J. L., Griggs, J. A., Hurkmans, R. T. W. L., Dowdeswell, J. A., Gogineni, S. P., Howat, I., Mouginot, J., Paden, J., Palmer, S., Rignot, E., and Steinhage, D.: A new bed elevation dataset for Greenland, *The Cryosphere*, 7, 499–510, <https://doi.org/10.5194/tc-7-499-2013>, 2013.
- Beamer, J. P., Hill, D. F., Arendt, A., and Liston, G. E.: High-resolution modeling of coastal freshwater discharge and glacier mass balance in the Gulf of Alaska watershed. *Water Resour. Res.*, 52, 3888–3909, doi:10.1002/2015WR018457, 2016.
- 535 Berends, C. J., de Boer, B., and van de Wal, R. S. W.: Application of HadCM3@Bristolv1.0 simulations of paleoclimate as forcing for an ice-sheet model, ANICE2.1: set-up and benchmark experiments, *Geoscientific Model Development* 11, 4657–4675, 2018.
- Bintanja, R., van de Wal, R. S. W., and Oerlemans, J.: Global ice volume variations through the last glacial cycle simulated by a 3-D ice-dynamical model, *Quaternary International* 95-96, 11-23, 2002.
- 540 Born, A., Imhof, M. A., and Stocker, T. F.: An efficient surface energy–mass balance model for snow and ice, *The Cryosphere*, 13, 1529–1546, <https://doi.org/10.5194/tc-13-1529-2019>, 2019.
- Bougamont, M., Bamber, J. L., Ridley, J. K., Gladstone, R. M., Greuell, W., Hanna, E., Payne, A. J., and Rutt, I.: Impact of model physics on estimating the surface mass balance of the Greenland ice sheet, *Geophys. Res. Lett.*, 34, L17501, doi:10.1029/2007GL030700, 2007.



- 545 Box, J. E.: Greenland ice sheet mass balance reconstruction. Part II: Surface mass balance (1840-2010), *J. Climate*, Vol. 26, No. 18, 6974-6989. doi:10.1175/JCLI-D-12-00518.1, 2013.
- Box, J. E., Fettweis, X., Stroeve, J. C., Tedesco, M., Hall, D. K., & Steffen, K.: Greenland ice sheet albedo feedback: thermodynamics and atmospheric drivers. *The Cryosphere*, 6(4), 821-839, 2012.
- Box, J.E., N. Cressie, D.H. Bromwich, J. Jung, M. van den Broeke, J.H. van Angelen, R.R. Forster, C. Miège, E. Mosley-  
550 Thompson, B. Vinther, J.R. McConnell: Greenland ice sheet mass balance reconstruction. Part I: net snow accumulation (1600-2009). *J. Climate*, 26, 3919–3934. doi:10.1175/JCLI-D-12-00373.1, 2013.
- Box, J.E., W. Colgan: Greenland ice sheet mass balance reconstruction. Part III: Marine ice loss and total mass balance (1840–2010). *Journal of Climate*, 26, 6990–7002. doi:10.1175/JCLI-D-12-00546.1, 2013.
- Braithwaite, R. J.: Calculation of sensible-heat flux over a melting ice surface using simple climate data and daily  
555 measurements of ablation, *Annals of Glaciology*, 50, 9–15, <https://doi.org/10.3189/172756409787769726>, 2009.
- Cappelen, J., B. V. Jørgensen, E. V. Laursen, L. S. Stannius, and R. S. Thomsen: The observed climate of Greenland, 1958–99 with climatological standard normals, 1961–90. Danish Meteorological Institute Tech. Rep. 00-18, 152 pp, 2001.
- Cappelen, J., E. V. Laursen, P. V. Jørgensen, and C. Kern-Hansen: DMI monthly climate data collection 1768–2005, Denmark, the Faroe Islands and Greenland. Danish Meteorological Institute Tech. Rep. 06-09, 53 pp, 2006.
- 560 Cappelen, J.: DMI monthly climate data collection 1768–2010, Denmark, the Faroe Islands and Greenland. Danish Meteorological Institute Tech. Rep. 11-05, 54 pp, 2011.
- de Boer, B., Stocchi, P., and van de Wal, R.: A fully coupled 3-D ice-sheet-sea-level model: algorithm and applications, *Geoscientific Model Development* 7, 2141-2156, 2014.
- Dee, D. P., Uppala, S. M., Simmons, A. J., Berrisford, P., Poli, P., Kobayashi, S., Andrae, U., Balmaseda, M. A., Balsamo, G.,  
565 Bauer, P., Bechtold, P., Beljaars, A. C. M., van de Berg, L., Bidlot, J., Bormann, N., Delsol, C., Dragani, R., Fuentes, M., Geer, A. J., Haimberger, L., Healy, S. B., Hersbach, H., Holm, E. V., Isaksen, L., Kållberg, P., Kohler, M., Matricardi, M., McNally, A. P., Monge-Sanz, B. M., Morcrette, J.-J., Park, B.-K., Peubey, C., de Rosnay, P., Tavolato, C., Thepaut, J.-N., Vitart, F.: The ERA-Interim reanalysis: configuration and performance of the data assimilation system. *Q. J. R. Meteorol. Soc.*, 137, 553–597, doi:10.1002/qj.828, 2011.
- 570 Delhasse, A., Fettweis, X., Kittel, C., Amory, C., and Agosta, C.: Brief communication: Impact of the recent atmospheric circulation change in summer on the future surface mass balance of the Greenland Ice Sheet, *The Cryosphere*, 12, 3409–3418, <https://doi.org/10.5194/tc-12-3409-2018>, 2018.
- Delhasse, A., Kittel, C., Amory, C., Hofer, S., and Fettweis, X.: Brief communication: Interest of a regional climate model against ERA5 to simulate the near-surface climate of the Greenland ice sheet, *The Cryosphere Discuss.*,  
575 <https://doi.org/10.5194/tc-2019-96>, in review, 2019.
- ECWMF-IFS: Part IV : Physical Processes (CY33R1), Tech. Rep. June, 2008.
- Ekholm, S.: A full coverage, high-resolution, topographic model of Greenland computed from a variety of digital elevation data. *J. Geophys. Res.* 101, 21961-21972, 1996.



- Ettema, J., M. R. van den Broeke, E. van Meijgaard, W. J. van de Berg, J. L. Bamber, J. E. Box, and R. C. Bales: Higher  
580 surface mass balance of the Greenland Ice Sheet revealed by high-resolution climate modeling. *Geophys. Res. Lett.*, 36,  
L12501, doi:10.1029/2009GL038110, 2009.
- Ettema, J., van den Broeke, M. R., van Meijgaard, E., van de Berg, W. J., Box, J. E., and Steffen, K.: Climate of the  
Greenland ice sheet using a high-resolution climate model – Part 1: Evaluation, *The Cryosphere*, 4, 511–527, <https://doi.org/10.5194/tc-4-511-2010>, 2010.
- 585 Fettweis, X., Box, J. E., Agosta, C., Amory, C., Kittel, C., Lang, C., van As, D., Machguth, H., and Gallée, H.:  
Reconstructions of the 1900–2015 Greenland ice sheet surface mass balance using the regional climate MAR model, *The  
Cryosphere*, 11, 1015–1033, <https://doi.org/10.5194/tc-11-1015-2017>, 2017.
- Fettweis, X., Franco, B., Tedesco, M., van Angelen, J. H., Lenaerts, J. T. M., van den Broeke, M. R., and Gallée, H.:  
Estimating the Greenland ice sheet surface mass balance contribution to future sea level rise using the regional atmospheric  
590 climate model MAR, *The Cryosphere*, 7, 469–489, <https://doi.org/10.5194/tc-7-469-2013>, 2013a.
- Fettweis, X., Hanna, E., Lang, C., Belleflamme, A., Ericum, M., and Gallée, H.: Brief communication "Important role of the  
mid-tropospheric atmospheric circulation in the recent surface melt increase over the Greenland ice sheet", *The Cryosphere*,  
7, 241–248, <https://doi.org/10.5194/tc-7-241-2013>, 2013b.
- Goelzer, H., Huybrechts, P., Furst, J., Nick, F., Andersen, M., Eswards, T., Fettweis, X., Payne, A., and Shannon, S.:  
595 Sensitivity of Greenland ice sheet projections to model formulations. *Journal of Glaciology*, 59(216), 733–749, 2013.
- Greuell, W.: Numerical Modelling of the Energy Balance and the Englacial Temperature at the ETH Camp, West  
Greenland, *Zürcher Geographische Schriften*, 51, 1–81, 1992.
- Hanna, E., P. Huybrechts, I. Janssens, J. Cappelen, K. Steffen, A. Stephens: Runoff and mass balance of the Greenland ice  
sheet: 1958–2003. *J. Geophys. Res.* 110 (D13), D13108, 2005.
- 600 Hanna, E., P. Huybrechts, J. Cappelen, K. Steffen, R.C. Bales, E. Burgess, J.R. McConnell, J.P. Steffensen, M. Van den  
Broeke, L. Wake, G. Bigg, M. Griffiths, D. Savas: Greenland Ice Sheet surface mass balance 1870 to 2010 based on  
Twentieth Century Reanalysis, and links with global climate forcing. *J. Geophys. Res.* 116, D24121, 2011.
- Hanna, E., Fettweis, X., and Hall, R. J.: Brief communication: Recent changes in summer Greenland blocking captured by  
none of the CMIP5 models, *The Cryosphere*, 12, 3287–3292, <https://doi.org/10.5194/tc-12-3287-2018>, 2018.
- 605 Hanna, E. and Pattyn, F. and Navarro, F. and Favier, V. and Goelzer, H. and van den Broeke, M.R. and Vizcaino, M. and  
Whitehouse, P.L. and Ritz, C. and Bulthuis, K. and Smith, B.: Mass balance of the ice sheets and glaciers – progress since  
AR5 and challenges, *Earth-science reviews*, <https://doi.org/10.1016/j.earscirev.2019.102976>, 2019.
- Hashimoto, A., Niwano, M., Aoki, T., Tsutaki, S., Sugiyama, S., Yamasaki, T., Iizuka, Y., and Matoba, S.: Numerical weather  
prediction system based on JMA-NHM for field observation campaigns on the Greenland ice sheet, *Low Temperature  
610 Science*, 75, 91–104, <https://doi.org/10.14943/lowtemsci.75.91>, 2017.
- Hofer, S., Tedstone, A.J., Fettweis, X. and J. Bamber. Cloud microphysics and circulation anomalies control differences in  
future Greenland melt. *Nat. Clim. Chang.* 9, 523–528, doi:10.1038/s41558-019-0507-8, 2019.



- Hofer, S., Tedstone, A. J., Fettweis, X. & Bamber, J. L. Decreasing cloud cover drives the recent mass loss on the Greenland Ice Sheet. *Science Advances* 3(6), e170058, 2017.
- 615 Huybrechts, P. and de Wolde, J.: The Dynamic Response of the Greenland and Antarctic Ice Sheets to Multiple-Century Climatic Warming, *Journal of Climate* 12, 2169-2188, 1999.
- IPCC: Summary for Policymakers. In: IPCC Special Report on the Ocean and Cryosphere in a Changing Climate [H.- O. Pörtner, D.C. Roberts, V. Masson-Delmotte, P. Zhai, M. Tignor, E. Poloczanska, K. Mintenbeck, M. Nicolai, A. Okem, J. Petzold, B. Rama, N. Weyer (eds.)], in press, 2019.
- 620 Janssens, I. and Huybrechts, P.: The treatment of meltwater retention in mass-balance parameterizations of the Greenland ice sheet, *Annals of Glaciology* 31, 133-140, 2000.
- Jowett, A., E. Hanna, F. Ng, P. Huybrechts, I. Janssens: A new spatially and temporally variable sigma parameter in degree-day melt modelling of the Greenland Ice Sheet 1870-2013. *The Cryosphere Discuss* 9. 5327-5371, 2015.
- King, M. D., Howat, I. M., Jeong, S., Noh, M. J., Wouters, B. and Noël, B.: Seasonal to decadal variability in ice discharge  
625 from the Greenland Ice Sheet, *Cryosph.*, 12, 3813–3825, 2018.
- Khan, S. A., Sasgen, I., Bevis, M., van Dam, T., Bamber, J. L., Wahr, J., Willis, M., Kjaer, K. H., Wouters, B., Helm, V., Csatho, B., Fleming, K., Bjork, A. A., Aschwanden, A., Knudsen, P., and Munneke, P. K.: Geodetic measurements reveal similarities between post-Last Glacial Maximum and present-day mass loss from the Greenland ice sheet, *Sci. Adv.*, 2, e1600931–e1600931, <https://doi.org/10.1126/sciadv.1600931>, 2016.
- 630 Kobayashi, S., Ota, Y., Harada, Y., Ebata, A., Moriya, M., Onoda, H., Onogi, K., Kamahori, H., Kobayashi, C., Endo, H., Miyaoka, K., and Takahashi, K.: The JRA-55 reanalysis: General specifications and basic characteristics, *J. Meteorol. Soc. Jpn.*, 93, 5–48, <https://doi.org/10.2151/jmsj.2015-001>, 2015.
- Krebs-Kanzow, U. Gierz, P., Lohmann, G.: Brief communication: An ice surface melt scheme including the diurnal cycle of solar radiation, *The Cryosphere*, 12, 3923–3930, <https://doi.org/10.5194/tc-12-3923-2018>, 2018.
- 635 Langen, P. L., Fausto, R.S., Vandecrux, B., Mottram R.H. and Box, J.E.: Liquid Water Flow and Retention on the Greenland Ice Sheet in the Regional Climate Model HIRHAM5: Local and Large-Scale Impacts, *Front. Earth Sci.*, 4:110, doi: 10.3389/feart.2016.00110, 2017.
- Lenaerts, J. T. M., van den Broeke, M. R., van Angelen, J. H., van Meijgaard, E., and Déry, S. J.: Drifting snow climate of the Greenland ice sheet: a study with a regional climate model, *The Cryosphere*, 6, 891–899, [https://doi.org/10.5194/tc-6-891-](https://doi.org/10.5194/tc-6-891-2012)  
640 2012, 2012.
- Lenaerts, J. T. M., Medley, B., van den Broeke, M. R., & Wouters, B.: Observing and modeling ice sheet surface mass balance. *Reviews of Geophysics*, 57, 376– 420. <https://doi.org/10.1029/2018RG000622>, 2019.
- Lewis, G., Osterberg, E., Hawley, R., Whitmore, B., Marshall, H. P., and Box, J.: Regional Greenland accumulation variability from Operation IceBridge airborne accumulation radar, *The Cryosphere*, 11, 773-788, doi:10.5194/tc-11-773-  
645 2017, 2017.



- Lewis, G., Osterberg, E., Hawley, R., Marshall, H. P., Meehan, T., Graeter, K., McCarthy, F., Overly, T., Thundercloud, Z., and Ferris, D.: Recent precipitation decrease across the western Greenland ice sheet percolation zone, *The Cryosphere*, 13, 2797–2815, <https://doi.org/10.5194/tc-13-2797-2019>, 2019.
- Ligtenberg, S. R. M., Kuipers Munneke, P., Noël, B. P. Y., and van den Broeke, M. R.: Brief communication: Improved  
650 simulation of the present-day Greenland firn layer (1960–2016), *The Cryosphere*, 12, 1643–1649, <https://doi.org/10.5194/tc-12-1643-2018>, 2018.
- Liston, G. E.: Local advection of momentum, heat, and moisture during the melt of patchy snow covers. *J. Appl. Meteorol.*, 34, 1705–1715, doi:10.1175/1520-0450-34.7.1705, 1995.
- Liston, G. E. and Sturm, M.: A snow-transport model for complex terrain. *J. Glaciol.*, 44, 498–516, 1998.
- 655 Liston, G. E., Winther, J.-G., Bruland, O., Elvehøy, H., and Sand, K.: Below surface ice melt on the coastal Antarctic ice sheet. *J. Glaciol.*, 45, 273–285, 1999.
- Liston, G. E. and Sturm, M.: Winter precipitation patterns in Arctic Alaska determined from a blowing-snow model and snow depth observations. *J. Hydrometeorol.*, 3, 646–659, 2002.
- Liston, G. E. and Elder, K.: A distributed snow-evolution modeling system (SnowModel). *J. Hydrometeorol.*, 7, 1259–1276,  
660 doi:10.1175/JHM548.1, 2006a.
- Liston, G. E. and Elder, K.: A meteorological distribution system for high-resolution terrestrial modeling (MicroMet). *J. Hydrometeorol.*, 7, 217–234, doi:10.1175/JHM486.1, 2006b.
- Liston, G. E., Haehnel, R. B., Sturm, M., Hiemstra, C. A., Berezovskaya, S., and Tabler, R. D.: Simulating complex snow distributions in windy environments using SnowTran-3D. *J. Glaciol.*, 53, 241–256, 2007.
- 665 Liston, G. E. and Hiemstra, C. A.: The changing cryosphere: pan-Arctic snow trends (1979–2009). *J. Clim.*, 24, 5691–5712, 2011.
- Liston, G. E. and Mernild, S. H.: Greenland freshwater runoff. Part I: a runoff routing model for glaciated and non-glaciated landscapes (HydroFlow). *J. Clim.*, 25(17), 5997–6014, doi:10.1029/2011JD016267, 2012.
- Machguth, H., Thomsen, H. H., Weidick, A., Abermann, J., Ahlström, A. P., Andersen, M. L., Andersen, S. B., Björk, A. A.,  
670 Box, J. E., Braithwaite, R. J., Bøggild, C. E., Citterio, M., Clement, P., Colgan, W., Fausto, R. S., Gleie, K., Hasholt, B., Hynek, B., Knudsen, N. T., Larsen, S. H., Mernild, S., Oerlemans, J., Oerter, H., Olesen, O. B., Smeets, C. J. P. P., Steffen, K., Stober, M., Sugiyama, S., van As, D., van den Broeke, M. R., and van de Wal, R. S.: Greenland surface mass balance observations from the ice sheet ablation area and local glaciers, *J. Glaciol.*, 62, 861–887, doi:10.1017/jog.2016.75, 2016.
- Mernild, S. H., Liston, G. E., Hasholt, B., and Knudsen, N. T.: Snow distribution and melt modeling for Mittivakkat Glacier,  
675 Ammassalik Island, SE Greenland. *Journal of Hydrometeorology*, 7, 808–824, 2006.
- Mernild, S. H. and G. E. Liston: Greenland freshwater runoff. Part II: Distribution and trends, 1960–2010. *Journal of Climate*, 25(17), 6015–6035, doi.org/10.1175/JCLI-D-11-00592.1, 2012.
- Mernild, S. H., Holland, D. M., Holland, D., Rosing-Asvid, A., Yde, J. C., Liston, G. E., and Steffen, K.: Freshwater flux and spatiotemporal simulated runoff variability into Ilulissat Icefjord, West Greenland, linked to salinity and temperature



- 680 observations near tidewater glacier margins obtained using instrumented ringed seals. *Journal of Physical Oceanography*, 45(5), 1426–1445, doi: 10.1175/JPO-D-14-0217.1, 2015.
- Morlighem, M., Williams, C. N., Rignot, E., An, L., Arndt, J. E., Bamber, J. L., Catania, G., Chauché, N., Dowdeswell, J. A., Dorschel, B., Fenty, I., Hogan, K., Howat, I. M., Hubbard, A., Jakobsson, M., Jordan, T. M., Kjeldsen, K. K., Millan, R., Mayer, L., Mouginot, J., Noël, B. P. Y., O’Cofaigh, C., Palmer, S., Rysgaard, S., Seroussi, H., Siegert, M. J., Slabon, P.,
- 685 Straneo, F., van den Broeke, M. R., Weinrebe, W., Wood, M., and Zinglensen, K. B.: BedMachine v3: Complete Bed Topography and Ocean Bathymetry Mapping of Greenland From Multibeam Echo Sounding Combined With Mass Conservation, *Geophysical Research Letters* 44, 11,051–11,061, 2017.
- Mouginot, J., Rignot, E., Bjørk, A., van den Broeke, M., Millan, R., Morlighem, M., Noël, B., Scheuchl, B., Wood, M.: Forty-six years of Greenland Ice Sheet mass balance from 1972 to 2018, *Proceedings of the National Academy of Sciences* May
- 690 2019, 116 (19) 9239–9244; DOI: 10.1073/pnas.1904242116, 2019.
- Müller, W. A., Jungclaus, J. H., Mauritsen, T., Baehr, J., Bittner, M., Budich, R., Bunzel, F., Esch, M., Ghosh, R., Haak, H., Ilyina, T., Kleine, T., Kornbluh, L., Li, H., Modali, K., Notz, D., Pohlmann, H., Roeckner, E., Stemmler, I., Tian, F., Marotzke J.: A higher-resolution version of the Max Planck Institute Earth System Model (MPI-ESM1.2-HR). *Journal of Advances in Modeling Earth Systems*, 10 (7). pp. 1383–1413. ISSN 1942-2466, 2018.
- 695 Niwano, M., Aoki, T., Kuchiki, K., Hosaka, M., Kodama, Y., Yamaguchi, S., Motoyoshi, H., and Iwata, Y.: Evaluation of updated physical snowpack model SMAP, *Bull. Glaciol. Res.*, 32, 65–78, <https://doi.org/10.5331/bgr.32.65>, 2014.
- Niwano, M., Aoki, T., Kuchiki, K., Hosaka, M., and Kodama, Y.: Snow Metamorphism and Albedo Process (SMAP) model for climate studies: Model validation using meteorological and snow impurity data measured at Sapporo, Japan, *J. Geophys. Res.*, 117, F03008, <https://doi.org/10.1029/2011JF002239>, 2012.
- 700 Niwano, M., Hashimoto, A., and Aoki, T., 2019: Cloud-driven modulations of Greenland ice sheet surface melt, *Sci. Rep.*, 9, 10380, <https://doi.org/10.1038/s41598-019-46152-5>, 2019.
- Niwano, M., T. Aoki, A. Hashimoto, S. Matoba, S. Yamaguchi, T. Tanikawa, K. Fujita, A. Tsushima, Y. Iizuka, R. Shimada, and M. Hori, 2018: NHM–SMAP: spatially and temporally high-resolution nonhydrostatic atmospheric model coupled with detailed snow process model for Greenland Ice Sheet, *The Cryosphere*, 12, 635–655, <https://doi.org/10.5194/tc-12-635-2018>,
- 705 2018.
- Noël, B., van de Berg, W. J., Machguth, H., Lhermitte, S., Howat, I., Fettweis, X., and van den Broeke, M. R.: A daily, 1 km resolution data set of downscaled Greenland ice sheet surface mass balance (1958–2015), *The Cryosphere*, 10, 2361–2377, <https://doi.org/10.5194/tc-10-2361-2016>, 2016.
- Noël, B., van de Berg, W. J., van Wessem, J. M., van Meijgaard, E., van As, D., Lenaerts, J. T. M., Lhermitte, S., Kuipers
- 710 Munneke, P., Smeets, C. J. P. P., van Ulf, L. H., van de Wal, R. S. W., and van den Broeke, M. R.: Modelling the climate and surface mass balance of polar ice sheets using RACMO2 – Part 1: Greenland (1958–2016), *The Cryosphere*, 12, 811–831, <https://doi.org/10.5194/tc-12-811-2018>, 2018.



- Noël B, van de Berg WJ, Lhermitte S, van den Broeke MR: Rapid ablation zone expansion amplifies north Greenland mass loss, *Sci Adv.*, 5(9):eaaw0123. doi: 10.1126/sciadv.aaw0123, 2019.
- 715 Nowicki, S. M. J., Payne, A., Larour, E., Seroussi, H., Goelzer, H., Lipscomb, W., Gregory, J., Abe-Ouchi, A., and Shepherd, A.: Ice Sheet Model Intercomparison Project (ISMIP6) contribution to CMIP6, *Geosci. Model Dev.*, 9, 4521–4545, <https://doi.org/10.5194/gmd-9-4521-2016>, 2016.
- Oerlemans, Johannes, and W.H. Knap. : A 1 Year Record of Global Radiation and Albedo in the Ablation Zone of Morteratschgletscher, Switzerland, *Journal of Glaciology*, 44 (147): 231–38, 1998.
- 720 Ohmura, A.: Precipitation, accumulation and mass balance of the Greenland ice sheet, *Zeitschrift für Gletscherkunde und Glazialgeologie* 35, 1-20, 1999.
- Pfeffer, W. T., M. F. Meier, and T. H. Illangasekare.: Retention of Greenland runoff by refreezing: Implications for projected future sea level change. *J. Geophys. Res.*, 96, 22 117– 22 124, 1991.
- Rae, J. G. L., Aðalgeirsdóttir, G., Edwards, T. L., Fettweis, X., Gregory, J. M., Hewitt, H. T., Lowe, J. A., Lucas-Picher, P.,  
725 Mottram, R. H., Payne, A. J., Ridley, J. K., Shannon, S. R., van de Berg, W. J., van de Wal, R. S. W., and van den Broeke, M. R.: Greenland ice sheet surface mass balance: evaluating simulations and making projections with regional climate models, *The Cryosphere*, 6, 1275–1294, <https://doi.org/10.5194/tc-6-1275-2012>, 2012.
- Reijmer, C. H., van den Broeke, M. R., Fettweis, X., Ettema, J., and Stap, L. B.: Refreezing on the Greenland ice sheet: a comparison of parameterizations, *The Cryosphere*, 6, 743–762, <https://doi.org/10.5194/tc-6-743-2012>, 2012.
- 730 Rignot, E., Velicogna, I., van den Broeke, M. R., Monaghan, A., and Lenaerts, J. T. M. ( 2011), Acceleration of the contribution of the Greenland and Antarctic ice sheets to sea level rise, *Geophys. Res. Lett.*, 38, L05503, doi:10.1029/2011GL046583, 2011.
- Roe, G. H. and Lindzen, R. S.: The Mutual Interaction between Continental-Scale Ice Sheets and Atmospheric Stationary Waves, *Journal of Climate* 14, 1450-1465, 2001.
- 735 Roe, G. H.: Modeling precipitation over ice sheets: an assessment using Greenland, *Journal of Glaciology* 48, 70-80, 2002.
- Rolstad, C. and Oerlemans, J.: The residual method for determination of the turbulent exchange coefficient applied to automatic weather station data from Iceland, Switzerland and West Greenland, *Annals of Glaciology*, 42, 367–372, <https://doi.org/10.3189/172756405781813041>, 2005.
- Ryan, J. C., Smith, L. C., Van As, D., Cooley, S. W., Cooper, M. G., Pitcher, L. H., & Hubbard, A.: Greenland Ice Sheet  
740 surface melt amplified by snowline migration and bare ice exposure. *Science advances*, 5(3), eaav3738, 2019.
- Saito, K., Fujita, T., Yamada, Y., Ishida, J., Kumagai, Y., Aranami, K., Ohmori, S., Nagasawa, R., Kumagai, S., Muroi, C., Kato, T., Eito, H., and Yamazaki, Y.: The operational JMA nonhydrostatic mesoscale model, *Mon. Weather Rev.*, 134, 1266–1298, <https://doi.org/10.1175/MWR3120.1>, 2006.
- Sasgen, I., van den Broeke, M., Bamber, J. L., Rignot, E., Sørensen, L. S., Wouters, B., Martinec, Z., Velicogna, I. and  
745 Simonsen, S. B.: Timing and origin of recent regional ice-mass loss in Greenland, *Earth Planet. Sci. Lett.*, 333–334, 293–303, doi:10.1016/j.epsl.2012.03.033, 2012.



- Screen, James A., and Ian Simmonds: The central role of diminishing sea ice in recent Arctic temperature amplification, *Nature* 464, 1334–1337, doi:10.1038/nature09051, 2010.
- Simmons, A. J. and Poli, P.: Arctic warming in ERA-Interim and other reanalyses, *Q. J. Roy. Meteorol. Soc.*, 141, 1147–  
750 1162, <https://doi.org/10.1002/qj.2422>, 2015.
- Steffen, K., J. Box: Surface climatology of the Greenland ice sheet: Greenland Climate Network 1995-1999. *J. Geophys. Res.* 106 (D24), 33951-33964, 2001.
- van Angelen, J. H., M. R. van den Broeke, and W. J. van de Berg: Momentum budget of the atmospheric boundary layer over the Greenland Ice Sheet and its surrounding seas. *J. Geophys. Res.*, 116, D10101, doi:10.1029/2010JD015485, 2011.
- 755 van de Berg, W. J. and Medley, B.: Brief Communication: Upper-air relaxation in RACMO2 significantly improves modelled interannual surface mass balance variability in Antarctica, *The Cryosphere*, 10, 459–463, <https://doi.org/10.5194/tc-10-459-2016>, 2016.
- Van den Broeke, M. R., Bamber, J., Ettema, J., Rignot, E., Schrama, E. J. O., van de Berg, W. J., van Meijgaard, E., Velicogna, I., and Wouters, B.: Partitioning recent Greenland mass loss, *Science*, 326, 984–986, 2009.
- 760 van den Broeke, M. R., Enderlin, E. M., Howat, I. M., Kuipers Munneke, P., Noël, B. P. Y., van de Berg, W. J., van Meijgaard, E., and Wouters, B.: On the recent contribution of the Greenland ice sheet to sea level change, *The Cryosphere*, 10, 1933–1946, <https://doi.org/10.5194/tc-10-1933-2016>, 2016.
- van den Broeke, M., Box, J., Fettweis, X., Hanna, E., Noël, B., Tedesco, M., van As, D., van de Berg, W. J., & van Kampenhout, L.: Greenland Ice Sheet Surface Mass Loss: Recent Developments in Observation and Modeling, *Current*  
765 *Climate Change Reports*, 3: 345. <https://doi.org/10.1007/s40641-017-0084-8>, 2017.
- Van de Wal, R.: Mass-balance modelling of the Greenland ice sheet: A comparison of an energy-balance and a degree-day model. *Annals of Glaciology*, 23, 36-45. doi:10.3189/S0260305500013239, 1996.
- van Kampenhout, L., Rhoades, A. M., Herrington, A. R., Zarzycki, C. M., Lenaerts, J. T. M., Sacks, W. J., and van den Broeke, M. R.: Regional grid refinement in an Earth system model: impacts on the simulated Greenland surface mass  
770 balance, *The Cryosphere*, 13, 1547–1564, <https://doi.org/10.5194/tc-13-1547-2019>, 2019.
- van Meijgaard, E., L. H. van Ulf, W. J. Van de Berg, F. C. Bosvelt, B. J. J. M. Van den Hurk, G. Lenderink, and A. P. Siebesma: The KNMI regional atmospheric model RACMO version 2.1. KNMI Tech. Rep. 302, 43 pp, 2008.
- Vernon, C. L., Bamber, J. L., Box, J. E., van den Broeke, M. R., Fettweis, X., Hanna, E., and Huybrechts, P.: Surface mass balance model intercomparison for the Greenland ice sheet, *The Cryosphere*, 7, 599–614, <https://doi.org/10.5194/tc-7-599-2013>, 2013.
- Vinther, B. M., K. K. Andersen, P. D. Jones, K. R. Briffa, and J. Cappelen: Extending Greenland temperature records into the late eighteenth century. *J. Geophys. Res.*, 111, D11105, doi:10.1029/2005JD006810, 2006.
- Vizcaíno, M., Mikolajewicz, U., Jungclaus, J., and Schurgers, G. : Climate modification by future ice sheet changes and consequences for ice sheet mass balance. *Clim. Dyn.*, 34: 301. doi:10.1007/s00382-009-0591-y, 2010.



- 780 Wilton, D.J., A. Jowett, E. Hanna, G.R. Bigg, M. van den Broeke, X. Fettweis, P. Huybrechts: High resolution (1 km) positive degree-day modelling of Greenland ice sheet surface mass balance, 1870-2012 using reanalysis data, *J. Glaciol.* 63, 176-193, 2017.
- Wouters, B., Chambers, D., & Schrama, E. J. O.: GRACE observes small-scale mass loss in Greenland. *Geophysical Research Letters*, 35(20), 2008.
- 785 Yamaguchi, S., Watanabe, K., Katsushima, T., Sato, A., and Kumakura, T.: Dependence of the water retention curve of snow on snow characteristics, *Ann. Glaciol.*, 53, 6–12, <https://doi.org/10.3189/2012AoG61A001>, 2012.
- Yang, K., Koike, T., Stackhouse, P., Mikovitz, C., and Cox, S. J.: An assessment of satellite surface radiation products for highlands with Tibet instrumental data. *Geophys. Res. Lett.*, 33, L22403. doi:10.1029/2006GL027640, 2006.
- Zolles, T. and Born, A.: Sensitivity of the Greenland mass and energy balance to uncertainties in key model parameters, *The Cryosphere Discuss.*, <https://doi.org/10.5194/tc-2019-251>, in review, 2019.
- 790



	ice cores (# 260; 0.33±0.08mWE)			Snow pits (#130; 0.41±0.34mWE)		
	Bias	RMSE	Correlation	Bias	RMSE	Correlation
BESSI (EBM)	-0.07	0.11	0.87	-0.11	0.38	0.72
BOX13 (RCM)	0.10	0.19	0.87	-0.03	0.33	0.73
CESM (GCM)	0.05	0.14	0.80	-0.16	0.41	0.67
dEBM (EBM)	-0.01	0.08	0.90	-0.12	0.44	0.43
HIRHAM (RCM)	0.02	0.13	0.83	-0.10	0.38	0.66
IMAU-ITM (EBM)	0.00	0.10	0.88	0.12	0.53	0.16
MAR (RCM)	0.01	0.08	0.93	-0.08	0.37	0.68
MPI-ESM (GCM)	0.01	0.12	0.76	-0.08	0.35	0.75
NHM-SMAP (RCM)	0.01	0.09	0.93	-0.10	0.30	0.81
PDD1km	-0.01	0.04	0.97	-0.09	0.44	0.40
PDD5km	-0.01	0.04	0.96	-0.09	0.46	0.27
RACMO (RCM)	-0.02	0.08	0.88	-0.12	0.36	0.78
SNOWMODEL (EBM)	-0.05	0.12	0.87	-0.17	0.47	0.33
<b>ENSEMBLE</b>	<b>0.00</b>	<b>0.06</b>	<b>0.95</b>	<b>-0.09</b>	<b>0.39</b>	<b>0.60</b>
	PROMICE - GrIS + ice caps (#1683; -0.84±0.61mWE)			PROMICE – main ice sheet (#1438; -0.92±0.62mWE)		
BESSI (EBM)	0.38	0.87	0.79	0.45	0.89	0.81
BOX13 (RCM)	0.24	0.86	0.77	0.23	0.86	0.78
CESM (GCM)	0.11	0.66	0.86	0.11	0.61	0.89
dEBM (EBM)	-0.06	0.64	0.87	-0.03	0.66	0.87
HIRHAM (RCM)	0.13	0.58	0.90	0.09	0.57	0.91
IMAU-ITM (EBM)	-0.02	0.60	0.88	0.03	0.58	0.89
MAR (RCM)	0.10	0.49	0.93	0.10	0.48	0.93
MPI-ESM (GCM)	-0.06	0.76	0.81	-0.05	0.69	0.85
NHM-SMAP (RCM)	0.40	0.77	0.89	0.39	0.78	0.88
PDD1km				-0.18	0.69	0.89
PDD5km				-0.17	0.72	0.86
RACMO (RCM)	-0.07	0.62	0.89	-0.05	0.63	0.90
SNOWMODEL (EBM)	-0.30	0.67	0.89	-0.32	0.61	0.92
<b>ENSEMBLE</b>				<b>0.05</b>	<b>0.46</b>	<b>0.94</b>

795 Table 1: Statistics (in mWE) of models vs SMB databases described in Section 3.



	Basin 1			Basin 2			Basin 3			Basin 4		
	RMSE	Corr.	Trend	RMSE	Corr.	Trend	RMSE	Corr.	Trend	RMSE	Corr.	Trend
BESSI	10.4	0.95	3.1	18.9	0.87	-4.9	20.4	0.97	-35.4	32.6	0.98	-62.8
BOX13	10.7	0.94	7.4	18.9	0.87	13	22.1	0.96	-35.8	32.1	0.98	-88.6
CESM	13.7	0.91	-5.4	23.6	0.79	-31.2	44	0.87	-38.8	41.2	0.97	-57.7
dEBM	10.7	0.94	13.1	17.5	0.88	10.8	18.5	0.97	-31.1	33.9	0.98	-36.1
HIRHAM	8.8	0.96	-7.4	17.7	0.89	4	15.6	0.98	-24.4	24.5	0.98	-48.9
IMAU-ITM	18.2	0.86	39.1	21.6	0.86	38.1	14.8	0.98	-29.6	28.8	0.98	-19.9
MAR	9.3	0.96	12.3	16.5	0.9	4.7	16.4	0.98	-40.1	26	0.98	-39.3
MPI-ESM	15.9	0.88	-9.2	30.7	0.64	-21	27	0.95	-16.3	56.4	0.94	4.5
NHM-SMAP	9.5	0.95	6	18.5	0.87	3.6	15.8	0.98	-19.1	25.5	0.98	-75.3
PDD1km	11.9	0.93	-5.8	17.6	0.88	-14.6	19.1	0.97	-12.7	30.5	0.98	0
PDD5km	11.8	0.93	8.5	15.2	0.91	2.3	19.6	0.97	-14.2	30.4	0.98	-5.3
RACMO	9.8	0.95	12	17.3	0.89	12.8	16.3	0.98	-18.2	26.3	0.98	-38.9
SNOWMODEL	18.7	0.86	66	27.2	0.81	89.7	13.8	0.98	-8.4	23.8	0.99	-17.8
<b>ENSEMBLE</b>	<b>10.5</b>	<b>0.95</b>	<b>10.5</b>	<b>16.7</b>	<b>0.89</b>	<b>12.3</b>	<b>16.8</b>	<b>0.98</b>	<b>-23.5</b>	<b>27.7</b>	<b>0.98</b>	<b>-40.3</b>
	Basin 5			Basin 6			Ice sheet					
	RMSE	Corr.	Trend	RMSE	Corr.	Trend	RMSE	Corr.	Trend			
BESSI	45.2	0.94	-41.4	17	0.99	16.2	95.5	0.98	-113.7			
BOX13	39.4	0.96	2.7	15	0.99	-14.5	84	0.99	-103.1			
CESM	51.4	0.93	-41.4	21.5	0.98	-8.9	95.7	0.98	-165.9			
dEBM	43.5	0.95	0.1	19.1	0.99	20.6	94.5	0.98	-9.9			
HIRHAM	26	0.98	-1.1	14.5	0.99	-21.5	54.2	0.99	-87.3			
IMAU-ITM	43.7	0.95	2.7	26.5	0.98	30.7	101.2	0.98	71.6			
MAR	26.8	0.98	6.7	14.2	0.99	-1	51.7	0.99	-42.4			
MPI-ESM	90.3	0.8	31	39.9	0.96	-29.8	193.6	0.94	-28.3			
NHM-SMAP	32.7	0.97	-52.6	17	0.99	-29.7	71.3	0.99	-153.4			
PDD1km	42.7	0.95	-19.9	18.7	0.99	11.4	93.5	0.98	-28			
PDD5km	40.6	0.95	-6.4	19.6	0.99	27.7	83.5	0.99	26.1			
RACMO	26.9	0.98	-4.5	14.6	0.99	-9.4	56.7	0.99	-34.3			
SNOWMODEL	43.3	0.95	85.8	23.7	0.98	79.2	93.3	0.98	304.2			
<b>ENSEMBLE</b>	<b>35.1</b>	<b>0.96</b>	<b>-3.6</b>	<b>16.2</b>	<b>0.99</b>	<b>9.6</b>	<b>73.2</b>	<b>0.99</b>	<b>-22.3</b>			

800 Table 2: Statistics of models (in which the signal coming from the ice discharge has been subtracted from SMB) vs GRACE for each basin and the whole ice sheet. The trend (in Gt/month) shows the linear trend that must be applied to match GRACE estimates. RMSE (root-mean-square error) and correlation are computed after having applied this trend to the modelled time series.



805

	bare ice area and SMB > STD/2	bare ice area and SMB < STD/2	- Agreement
BESSI	3.5	1.1	95.5
BOX13	0.9	5.0	94.0
CESM	1.9	1.6	96.4
dEBM	0.6	2.9	96.4
HIRHAM	0.6	2.4	97.0
IMAU-ITM	0.5	9.2	90.4
MAR	0.4	3.6	96.0
MPI-ESM	0.8	2.3	96.9
NHM-SMAP	0.6	3.7	95.8
PDD1km	1.4	2.3	96.3
PDD5km	1.0	5.3	93.7
RACMO	0.7	3.0	96.3
SNOWMODEL	0.3	14.1	85.6
<b>ENSEMBLE</b>	<b>0.4</b>	<b>4.2</b>	<b>95.3</b>

**Table 3:** left) Percentage of the main ice sheet area where presence of bare ice area detected in MODIS on average over 2000-2012 and where the modelled mean SMB is significantly positive. The half of the interannual variability is used to evaluate the statistical significance of the equilibrium line. Middle) the same for (no) presence of bare ice and where SMB is significantly negative. Right) Percentage of agreement between modelled ablation zone and bare ice area from MODIS.

815



	SMB			Snowfall			Runoff		
	Mean	Std dev	Trend	Mean	Std dev	Trend	Mean	Std dev	Trend
BESSI	387	80	-4.1	566	54	0.3	134	52	4.2
BOX13	426	99	-6.5	718	61	-0.3	508	118	9.1
CESM	421	87	-3.1	668	59	0.1	276	66	4.0
dEBM	359	121	-8.1	604	59	-0.1	280	108	8.6
HIRHAM	398	109	-7.3	701	63	-1.5	491	123	8.2
IMAU-ITM	281	129	-8.7	638	62	0.4	382	122	9.5
MAR	372	122	-7.8	640	55	-0.5	302	107	8.0
MPI-ESM	284	101	-3.5	558	59	0.5	336	70	4.0
NHM-SMAP	429	99	-4.3	807	81	1.3	260	79	6.1
PDD1km	332	101	-6.3	519	55	0.2	230	87	7.0
PDD5km	285	111	-6.8	534	56	0.3	278	97	7.5
RACMO	357	115	-7.2	667	59	-0.7	306	90	6.7
SNOWMODEL	96	179	-12.9	665	65	0.3	469	171	13.4
<b>ENSEMBLE</b>	<b>338</b>	<b>111</b>	<b>-7.3</b>	<b>642</b>	<b>59</b>	<b>0.0</b>	<b>331</b>	<b>102</b>	<b>8.0</b>

Table 4: Mean, interannual variability (standard deviation of the annual means) and linear trend of the main ice sheet SMB, snowfall and runoff in (Gt/yr) over 1980-2012 simulated by the 13 models.

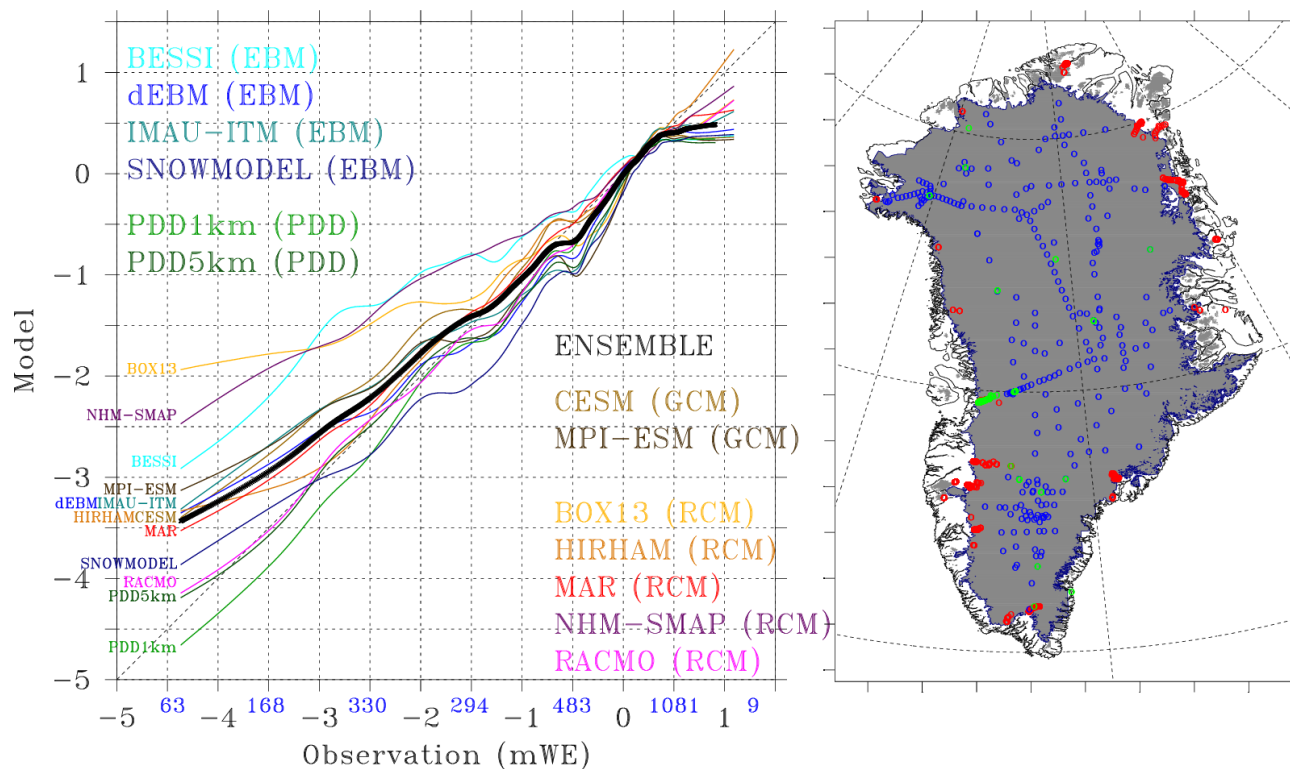
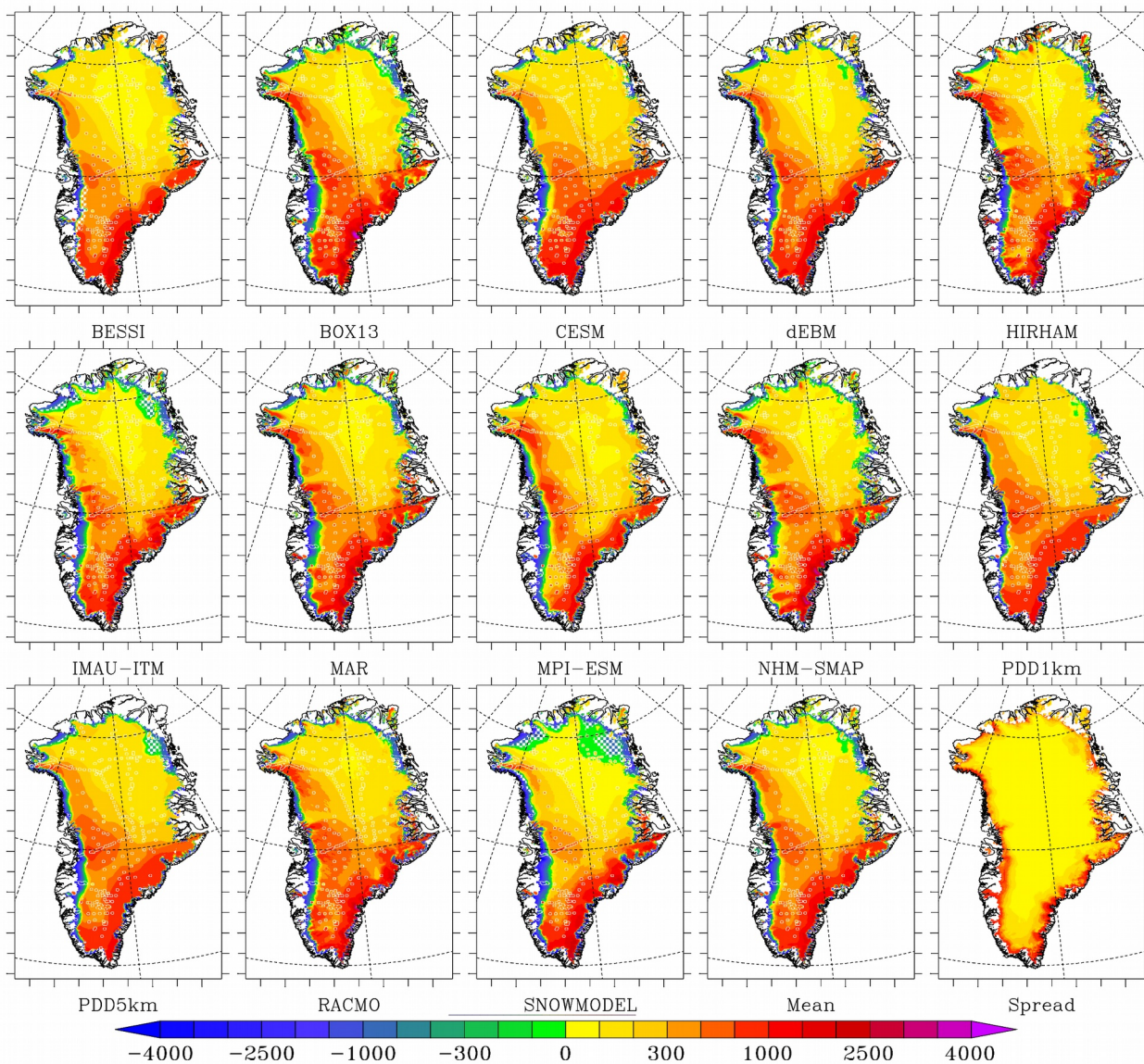


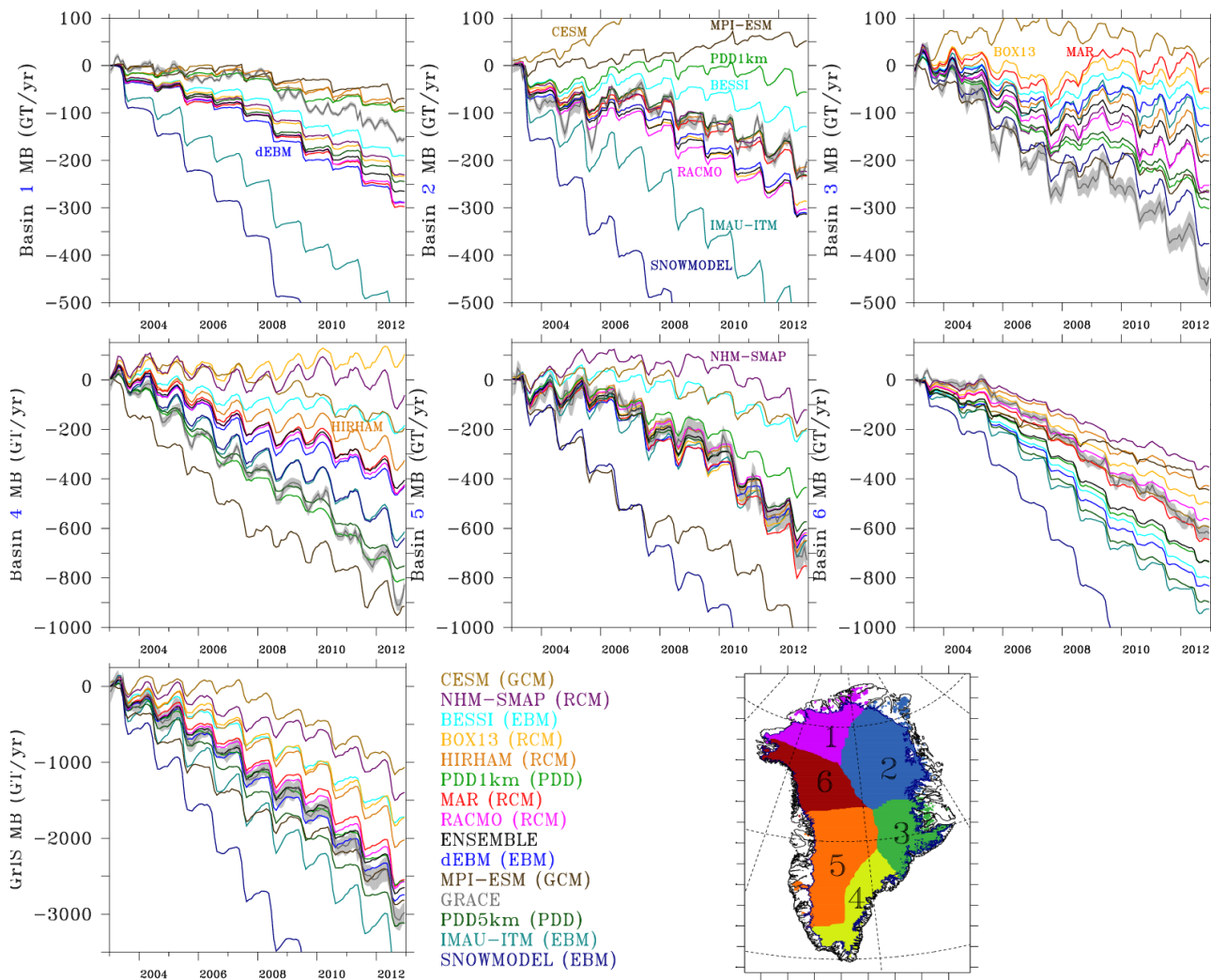
Fig. 1: Left) Scatter plot of modelled vs measured SMB in mWE. To increase the visibility of this figure, a running mean on 200 samples has been applied here after having sorted the samples (observation, model) on the observations. The numbers in blue on the X-axis indicate the number of observations with SMB values within each interval of the X-axis. Right) Locations of the in-situ measurements: ice cores in blue, snow pits in green and PROMICE in red.

825



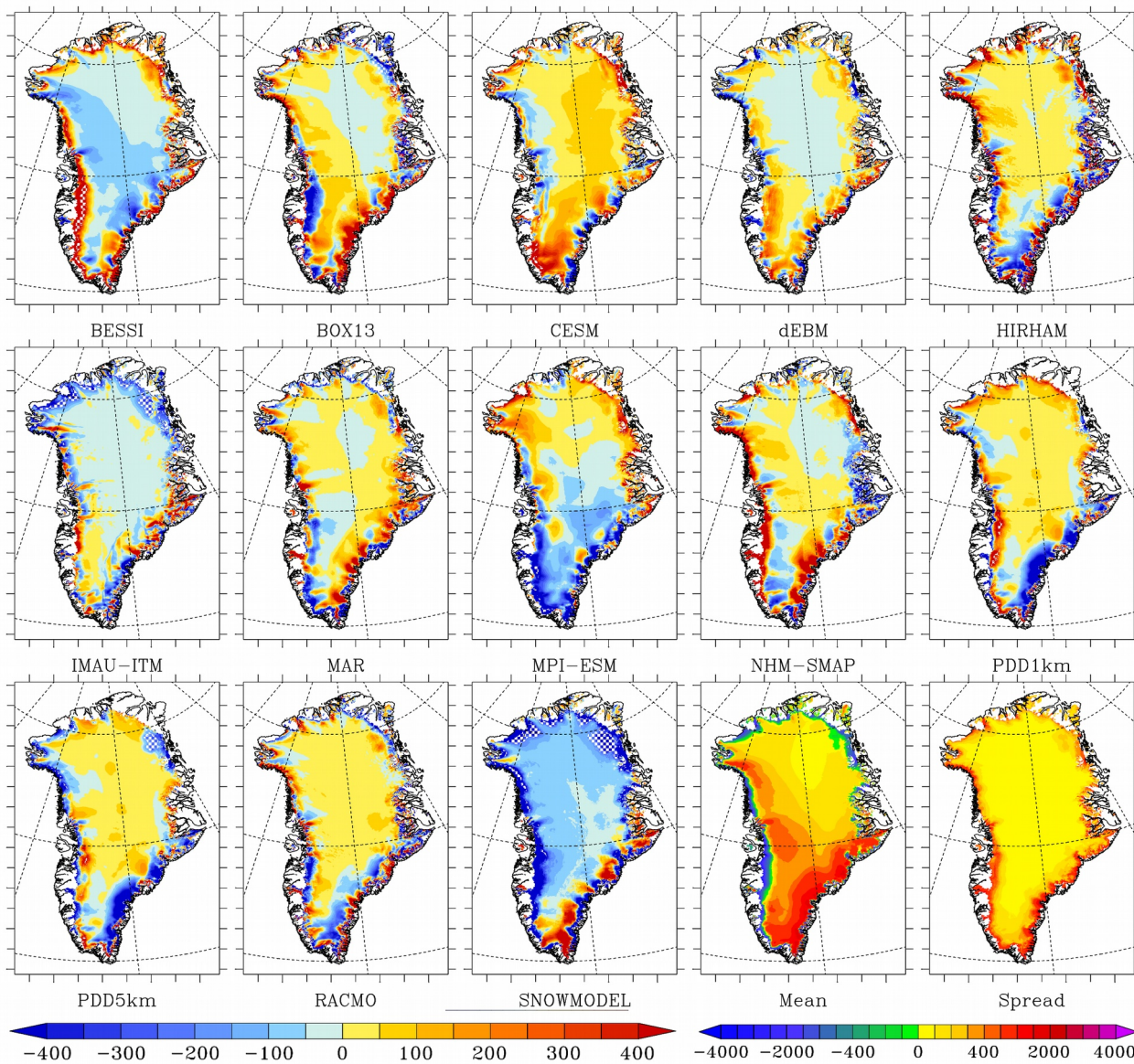
830 **Fig. 2: Mean SMB (in mmWE/yr) over 1980-2012 simulated by the 13 models as well as the ensemble model mean and the spread**  
**around this mean. The SMB measurements (ice cores + PROMICE) used to evaluate the models are represented as white circles. The**  
**areas listed in Table 3 where SMB disagree with the satellite derived bare ice area are shown in hatch. Finally, it is important to note**  
**that for better visibility, the scale is not linear by using a step of 100 for absolute values lower than 500 mmWE/yr and a step of 500**  
**above.**

835



840 **Fig. 3:** Time series of the mass balance (MB) changes from GRACE over 2003-2013 as well as from the 13 models in which the  
 signal from ice discharge (King et al., 2018) has been subtracted from the modelled SMB. Times series are shown for 6 basins  
 as well as over the whole ice sheet. Except for both PDD models, the ice caps from the common ice sheet mask are included and the  
 tundra areas are discarded. Finally, the legend is sorted in order of the mass balance changes estimated over the whole ice sheet.

845



850 Fig. 4: Same as Fig 2 but for the modelled SMB vs the ensemble model mean over 1980-2012 (shown in the 2 last plots). As Fig. 2, the areas listed in Table 3 where SMB disagrees with the MODIS-derived bare ice area are shown in hatch.

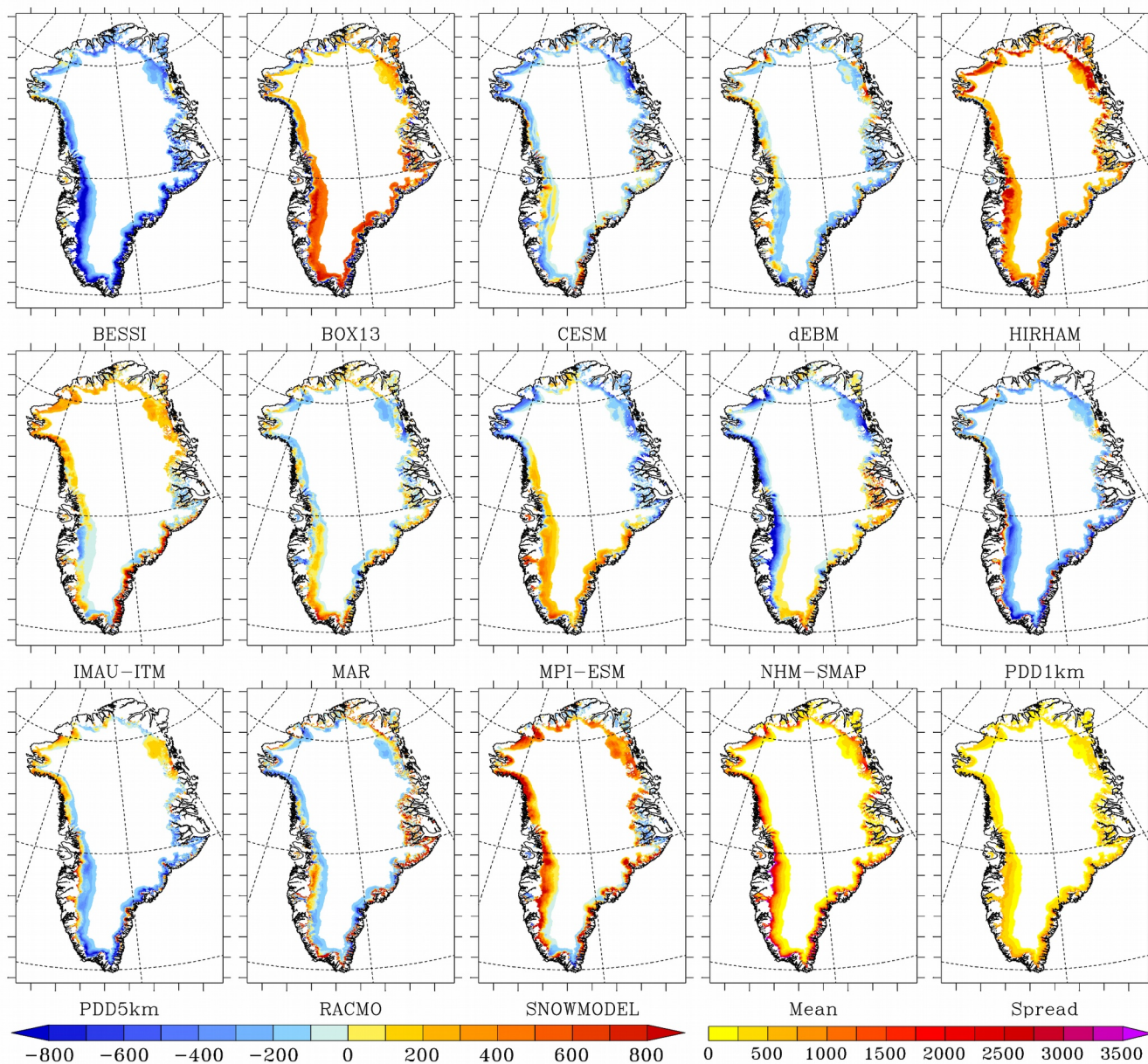
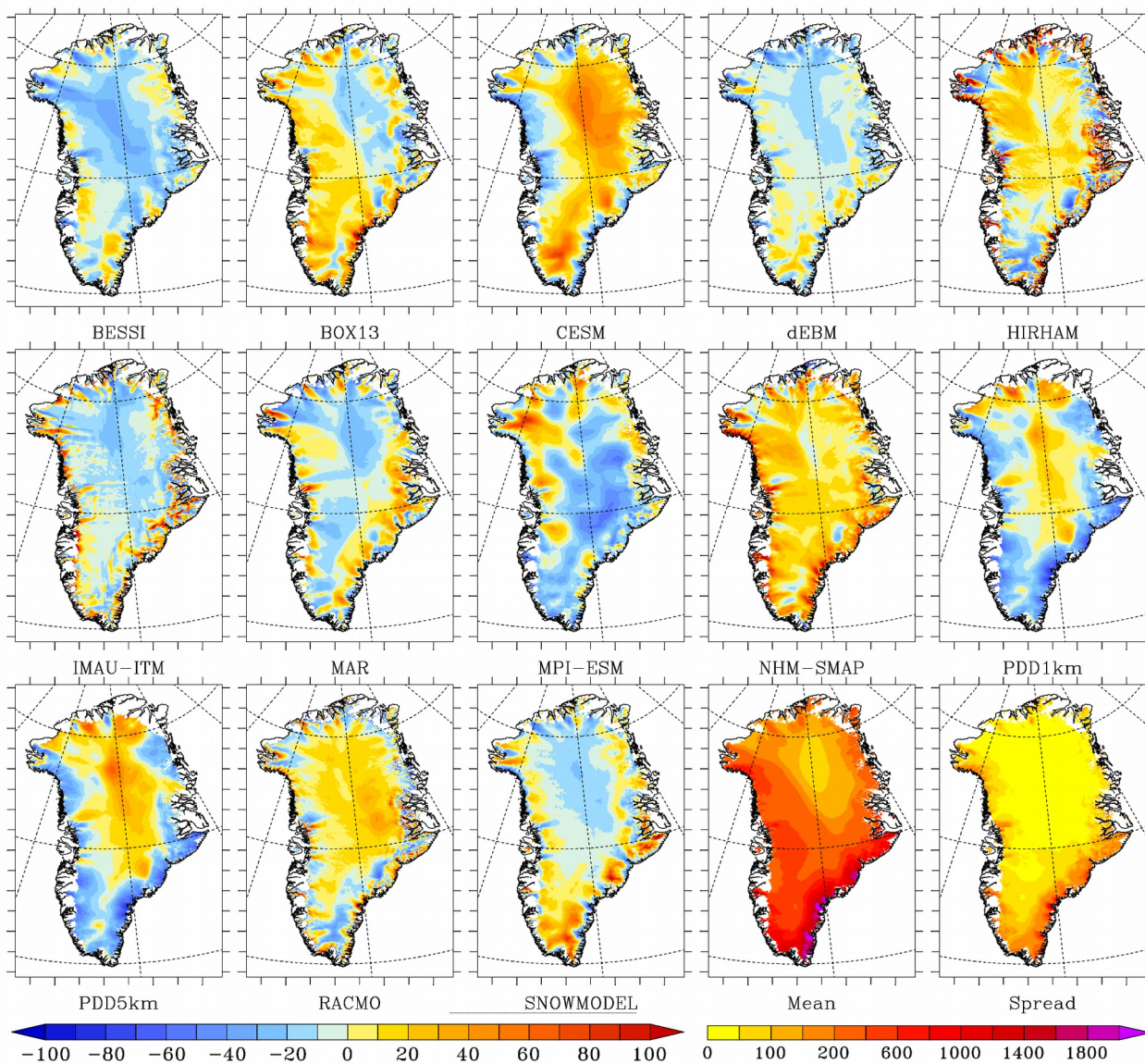


Fig. 5: Same as Fig 4 but for the modelled runoff. The ensemble mean and models spread around the mean are also shown in mmWE/yr in the two last plots. Finally it is important to note that only the area where the runoff of the ensemble mean is higher than 100mmWE/yr is shown here.

855



**Fig. 6:** Same as Fig 4 but for the modelled snowfall (linearly interpolated on the 1 km common grid but without any elevation correction) vs the ensemble model mean over 1980-2012 as a percentage of the ensemble model mean of snowfall accumulation. The ensemble mean and models spread around the mean are also shown in mmWE/yr in the two last plots.